Gut Dysbiosis during Influenza Contributes to Pulmonary Pneumococcal Superinfection through Altered Short-Chain Fatty Acid Production

Valentin Sencio, Adeline Barthélémy, Luciana Tavares, Marina Machado, Daphnée Soulard, Céline Cuinat, Celso Martins Queiroz-Junior, Marie-Louise Noordine, Sophie Salomé-Desnoulez, Lucie Deryuter, et al.

Article

Cell Reports

Gut Dysbiosis during Influenza Contributes to Pulmonary Pneumococcal Superinfection through Altered Short-Chain Fatty Acid Production

Graphical Abstract

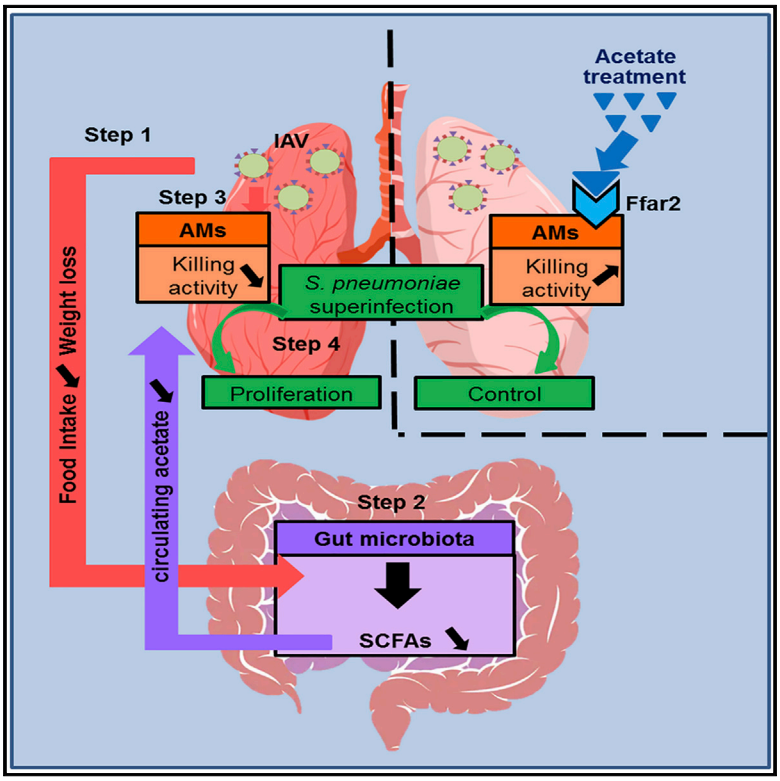

Highlights

- Influenza alters the production of SCFAs by the gut microbiota
- The dysbiotic microbiota transfers susceptibility to respiratory bacterial infection
- Supplementation with acetate restores the killing activity of alveolar macrophages
- Activation of the SCFA receptor FFAR2 protects against bacterial superinfection

Authors

Valentin Sencio, Adeline Barthelemy, Luciana P. Tavares, ..., Stéphanie Ferreira, Mauro M. Teixeira, François Trottein

Correspondence

francois.trottein@pasteur-lille.fr

In Brief

Sencio et al. provide insights into the mechanisms that underlie bacterial superinfection post-influenza. The authors demonstrate that influenza infection remotely alters the production of short-chain fatty acids (SCFAs) by the gut microbiota. Supplementation with acetate or pharmacological activation of the SCFA receptor FFAR2 reduces susceptibility to secondary bacterial infection.

Sencio et al., 2020, Cell Reports *30*, 2934–2947
March 3, 2020
https://doi.org/10.1016/j.celrep.2020.02.013

CellPress

OPEN ACCESS
CellPress

Cell Reports
Article

Gut Dysbiosis during Influenza Contributes to Pulmonary Pneumococcal Superinfection through Altered Short-Chain Fatty Acid Production

Valentin Sencio,[1,2,3,4,5] Adeline Barthelemy,[1,2,3,4,5] Luciana P. Tavares,[6] Marina G. Machado,[1,2,3,4,5,6] Daphnée Soulard,[1,2,3,4,5] Céline Cuinat,[7] Celso Martins Queiroz-Junior,[6] Marie-Louise Noordine,[7] Sophie Salomé-Desnoulez,[1,2,3,4,5] Lucie Deryuter,[1,2,3,4,5] Benoit Foligné,[8] Céline Wahl,[9] Benoit Frisch,[10] Angelica T. Vieira,[6] Christophe Paget,[1,2,3,4,5] Graeme Milligan,[11] Trond Ulven,[12] Isabelle Wolowczuk,[1,2,3,4,5] Christelle Faveeuw,[1,2,3,4,5] Ronan Le Goffic,[13] Muriel Thomas,[7] Stéphanie Ferreira,[9,14] Mauro M. Teixeira,[6,14] and François Trottein[1,2,3,4,5,15,*]

[1]Université de Lille, U1019 UMR 9017, Centre d'Infection et d'Immunité de Lille (CIIL), 59000 Lille, France
[2]Centre National de la Recherche Scientifique, UMR 9017, 59000 Lille, France
[3]Institut National de la Santé et de la Recherche Médicale, U1019, 59000 Lille, France
[4]Centre Hospitalier Universitaire de Lille, 59000 Lille, France
[5]Institut Pasteur de Lille, 59000 Lille, France
[6]Instituto de Ciências Biológicas, Universidade Federal de Minas Gerais, Belo Horizonte, Brazil
[7]Micalis Institute, Institut national de recherche pour l'agriculture, l'alimentation et l'environnement, AgroParisTech, Université Paris-Saclay, 78350 Jouy-en-Josas, France
[8]Université de Lille, Institut National de la Santé et de la Recherche Médicale (INSERM), CHU Lille, U995, Lille Inflammation Research International Center (LIRIC), 59000 Lille, France
[9]Genoscreen, 59000 Lille, France
[10]Centre National de la Recherche Scientifique, Université de Strasbourg, Faculté de Pharmacie, 67400 Illkirch, France
[11]Centre for Translational Pharmacology, Institute of Molecular, Cell and Systems Biology, University of Glasgow, G12 8QQ Glasgow, Scotland, UK
[12]Department of Pharmacology, University of Copenhagen, 2100 Copenhagen, Denmark
[13]Molecular Virology and Immunology, Institut National de la Recherche Agronomique, Université Paris-Saclay, 78350 Jouy-en-Josas, France
[14]These authors contributed equally
[15]Lead Contact
*Correspondence: francois.trottein@pasteur-lille.fr
https://doi.org/10.1016/j.celrep.2020.02.013

SUMMARY

Secondary bacterial infections often complicate viral respiratory infections. We hypothesize that perturbation of the gut microbiota during influenza A virus (IAV) infection might favor respiratory bacterial superinfection. Sublethal infection with influenza transiently alters the composition and fermentative activity of the gut microbiota in mice. These changes are attributed in part to reduced food consumption. Fecal transfer experiments demonstrate that the IAV-conditioned microbiota compromises lung defenses against pneumococcal infection. In mechanistic terms, reduced production of the predominant short-chain fatty acid (SCFA) acetate affects the bactericidal activity of alveolar macrophages. Following treatment with acetate, mice colonized with the IAV-conditioned microbiota display reduced bacterial loads. In the context of influenza infection, acetate supplementation reduces, in a free fatty acid receptor 2 (FFAR2)-dependent manner, local and systemic bacterial loads. This translates into reduced lung pathology and improved survival rates of double-infected mice. Lastly, pharmacological activation of the SCFA receptor FFAR2 during influenza reduces bacterial superinfection.

INTRODUCTION

Despite the widespread application of vaccination programs and antiviral drug treatments, influenza A virus (IAV) infections are responsible for significant morbidity and mortality. Influenza infections can also result in sporadic and often devastating pandemics; the 1918 pandemic led to the death of 50 million people. Severe bacterial infections can occur in the aftermath of IAV infection and contribute significantly to the excess morbidity and mortality of influenza (McCullers, 2014). *Streptococcus pneumoniae* was the most commonly detected bacteria in the 1918 and 2009 influenza pandemics. Murine models have shown that infection with IAV disrupts pulmonary barrier integrity and dampens innate antibacterial immunity, thus favoring local bacterial outgrowth and dissemination from the lungs (Ballinger and Standiford, 2010; McCullers, 2014; Rynda-Apple et al., 2015; Short et al., 2014). This inability to control bacterial infection is associated with changes in the numbers and/or functions of innate immune cells, including alveolar macrophages, conventional dendritic cells, neutrophils, and non-conventional T cells

(Barthelemy et al., 2017; Ghoneim et al., 2013; McNamee and Harmsen, 2006; Sun and Metzger, 2014). Regarding the importance of the gut-lung axis in diseases (Budden et al., 2017; McAleer and Kolls, 2018), we hypothesized that perturbation of the gut microbiota during IAV infection might favor bacterial superinfection.

The gastrointestinal tract hosts a complex, highly diverse microbial ecosystem. The tightly regulated interplay between the microbiota and the host enables the establishment and persistence of immune homeostasis (Blander et al., 2017; Maslowski and Mackay, 2011; Thaiss et al., 2016). The impact of commensal microbes on host immune responses is not limited to the gut compartment (i.e., barrier functions and gut homeostasis) but also extends to systemic compartments and distant mucosal interfaces, such as the lungs (Budden et al., 2017; McAleer and Kolls, 2018). The mechanism by which the gut microbiota regulates the size and/or the functions of the steady-state immune cell pool depends on microbial-associated molecular patterns, microbial metabolites, and their interactions with progenitor cells and mature immune cells (Arpaia et al., 2013; Koh et al., 2016; Shapiro et al., 2014). It has recently been shown that a healthy microbiota has a critical role in the host's defense against respiratory tract infections, including IAV (Abt et al., 2012; Bradley et al., 2019; Ichinohe et al., 2011; Moriyama and Ichinohe, 2019; Steed et al., 2017) and *S. pneumoniae* (Brown et al., 2017; Clarke et al., 2010; Schuijt et al., 2016). In the latter context, nucleotide-binding oligomerization domain (NOD)-like receptor agonists modulate the functions of effector immune cells, including alveolar macrophages and neutrophils.

Pathological situations (such as infections and chronic inflammatory or metabolic disorders) can modify the diversity and composition of the gut microbiota, leading to dysbiosis (Levy et al., 2017). Changes in intestinal bacterial communities can influence disease outcomes even in distant organs, as demonstrated by transfer experiments with dysbiotic microbiota. Only a few studies have investigated the impact of an acute respiratory infection on the gut microbiota, and most of these involved animal (murine) models of influenza. In this system, severe infections with H1N1 and H5N1 IAV were associated with alteration of the gut microbiota (Bartley et al., 2017; Deriu et al., 2016; Groves et al., 2018; Wang et al., 2014a; Yildiz et al., 2018), a finding that seems also to apply to infections in humans (Qin et al., 2015). This perturbation of the microbiota is associated with enhanced susceptibility to secondary enteric infections (Deriu et al., 2016; Yildiz et al., 2018). Influenza-associated dysbiosis has yet to be fully characterized (e.g., metabolic output) and functionally explored. In particular, it remains to be seen whether changes in the composition of the gut microbiota during influenza infection affect remote (respiratory tract) bacterial infections. In the present study, we found that sublethal infection with the H3N2 and H1N1 subtypes of influenza is associated with changes in the composition of the gut (cecal and intestinal) microbiota and with a drop in the production of short-chain fatty acids (SCFAs), the end products of dietary fiber fermentation. Pair-feeding experiments indicate that this phenomenon was probably due to decreased food intake, a well-known feature of influenza (Monto et al., 2000). Fecal transfer experiments demonstrated that the alterations in the microbiota compromised pulmonary immunity against pneumococcal infection. We discovered that the diminished production of acetate (the predominant SCFA), by altering the bactericidal activity of alveolar macrophages, was responsible for this remote effect. Acetate supplementation during influenza infection reinforced, in a free fatty acid receptor 2 (FFAR2)-dependent manner, lung defenses against secondary pneumococcal infection and reduced the lethal outcome of superinfected mice. Lastly, activation of FFAR2 by a highly specific agonist mimicked the effects of acetate and protected against post-influenza bacterial superinfection. Our results provide new insights into the pathophysiological mechanisms that underlie secondary bacterial infection post-influenza and might be of value in developing appropriate therapeutic approaches in diseases associated with dysbiosis and secondary bacterial infections.

RESULTS

Sublethal Influenza Infection Transiently Alters the Composition and Metabolic Output of the Gut Microbiota

To study the impact of a sublethal influenza infection on the composition and functionality of the gut microbiota, feces from IAV (H3N2)-infected mice were collected, and 16S rRNA gene profiling was performed. The determination of the weighted phylogenetic UniFrac distance (beta diversity) using unsupervised clustering and principal-component analysis (PCA) clearly indicated an intergroup difference in the fecal microbiota at day 7 post-infection (7 dpi), but not at 14 dpi (Figure 1A). A taxonomic analysis did not reveal any major changes at the phylum level at 7 dpi, with the exception of the Verrucomicrobia (*Akkermansia*) and, to a lesser extent, the Cyanobacteria (Figure S1A; Table S1). Greater changes were observed for lower taxonomic affiliations. Within the Bacteroidetes phylum, the relative abundance of the *Bacteroidales S24-7* family was reduced, while that of the *Parabacteroidetes* and *Odoribacter* genera was enhanced at 7 dpi (Table S1). In the Firmicutes phylum, we observed a greater relative abundance of *Clostridiales* (unaffiliated), *Ruminococcaceae*, and *Mogibacteriacecea* families and the *Coprococcus*, *Roseburia*, *Defluvittalea*, *Dorea*, *Ruminococcus*, and *Gemmiger* genera (Figure S1B). In contrast, lower relative abundances were observed for the *Lachnospiraceae* family (mainly unaffiliated *Lachnospiraceae* and *Clostridium* genera) and the *Dehalobacterium* and *Lactobacillus* (*Bacilli* class) genera. Lastly, within the Proteobacteria phylum, the proportion of *Alphaproteobacteria* and *Gammaproteobacteria* (*Escherichia* genus) classes increased, while that of *Betaproteobacteria* (*Sutterella* genus) decreased. Unsupervised clustering and PCA of the cecal samples also revealed a clear shift at 7 dpi relative to the controls (mock-treated mice) (Figure 1B). Likewise, we observed variations at the phylum level and below (Table S2). It is noteworthy that along with increased relative abundances of Verrucomicrobia and Cyanobacteria (as was the case in feces), we observed a dramatic drop in Actinobacteria (*Bifidobacteriaceae* and *Coriobacteriaceae* families) in the cecal samples. Quantitative PCR assays did not reveal significant differences in the 16S rRNA gene copy number in the feces and cecal compartment at any of the time points post-influenza,

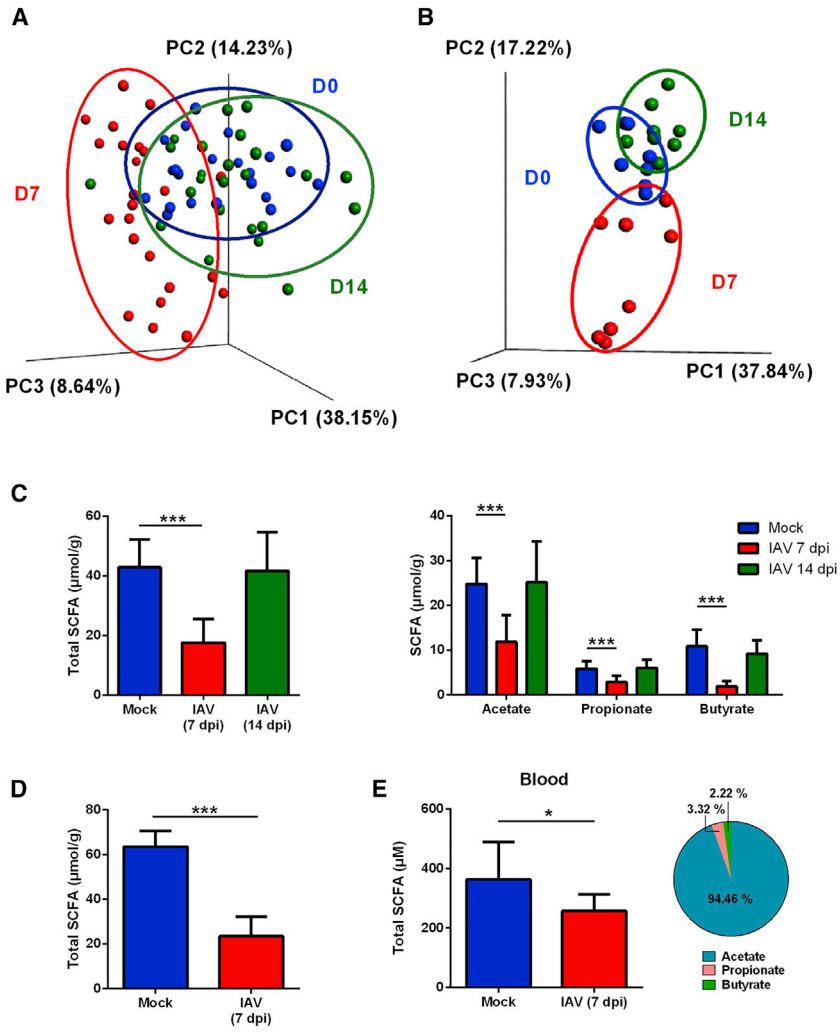

Figure 1. Altered Composition and Fermentative Activity (SCFA Production) of the Gut Microbiota during IAV Infection

(A) Seven and fourteen days after IAV (H3N2) infection, fecal contents were collected for 16S rDNA profiling. Fecal samples from each mouse were also collected the day of infection (D0). Bacterial communities were clustered using PCA of weighted UniFrac distance matrices (beta diversity). The first three principal coordinates (PC1, PC2, and PC3) are plotted for each sample, and the percentage variation in the plotted principal coordinates is indicated on the axes. Each spot represents one sample, and each group of mice is denoted by a different color (blue: noninfected/day 0, red: 7 dpi/day 7, green, 14 dpi/day 14). Distance between dots represents extent of compositional difference.

(B) PCA (H3N2/cecum). Blue, noninfected (mock); red, 7 dpi; green, 14 dpi (n = 8, one of three independent experiments shown).

(C) Cecal concentrations of total (left panel) and individual (right panel) SCFAs in mock-treated and IAV-infected mice (n = 21–33, five pooled experiments).

(D) Cecal concentrations of total SCFAs in mock-treated and IAV (H1N1/pdm09)-infected mice (7 dpi) (n = 6–8, one experiment performed).

(E) Blood concentrations of total SCFAs (9–10 pooled sera, 4 mice/pool). The repartition of individual SCFAs in the blood is represented (mock).

Results are expressed as the mean ± SD (C–E). Significant differences were determined using the Kruskal-Wallis ANOVA test (C) and the Mann-Whitney U test (D and E) (*$p < 0.05$; ***$p < 0.001$). See also Figures S1–S3 and Tables S1–S3.

demonstrating an overall stable gut bacterial load (Figure S1C). In line with other studies (Wang et al., 2014a; Yildiz et al., 2018), no IAV RNA genome was detected by quantitative PCR in the intestine of IAV-infected mice (Figure S1D). This suggests that dysbiosis was not due to viral replication in this site or to passive transport of viral RNA into the intestinal tissue. To expand upon these observations, we tested whether H1N1 IAV, which is the other dominant subtype in human IAVs, alters the composition of the gut microbiota. Infection with H1N1 IAVs also led to clear variations in the microbiota at 7 dpi (Figures S2 and S3; Tables S3 and S4). Similar changes in phylogenetic specifications were observed for H1N1-infected and H3N2-infected animals; shifts in *Bacteroidales S24-7*, *Lachnospiraceae*, *Ruminococcus*, *Lactobacillus*, *Sutterella*, and *Akkermansia* (relative to controls) were observed for both virus subtypes. Collectively, sublethal influenza (H3N2 and H1N1) infection leads to transient gut dysbiosis.

Since changes in the composition of the gut microbiota can alter its functionality (e.g., metabolic activity), we quantified the production of SCFAs, major metabolites of the gut microbiota, during the course of influenza infection. SCFAs are generated by bacterial fermentation of colonic dietary fibers, reaching high concentrations in the gut lumen under physiological conditions (Koh et al., 2016). As shown in Figure 1C (left panel), the total SCFA concentration in the cecum 7 days after H3N2 infection was lower relative to noninfected mice. The concentrations of acetate (the predominant SCFA), propionate, and butyrate were all lower (Figure 1C, right panel). At 14 dpi, the cecal SCFA concentrations returned to basal levels. A significantly reduced concentration of SCFAs was also observed at 7 dpi in mice infected with H1N1 IAV (Figure 1D). It is known that SCFAs produced in the gut can pass into the systemic circulation and then exert remote biological effects (particularly acetate and, to a lesser extent, propionate and butyrate) (Cait et al., 2018; Macia et al., 2015; Trompette et al., 2014). As seen in Figure 1E, influenza infection resulted in a lowered concentration of SCFAs in the blood at 7 dpi. In agreement with other studies (Cait et al., 2018; Macia et al., 2015; Mariño et al., 2017; Trompette et al., 2014), acetate was the predominant SCFA found in the blood. These data show that influenza infection alters the metabolic (fermentative) output of the gut microbiota at 7 dpi and that it affects local (gut) and systemic (blood) concentration of SCFAs, an emerging group of dietary derived metabolites endowed with immune regulatory functions (Tan et al., 2014).

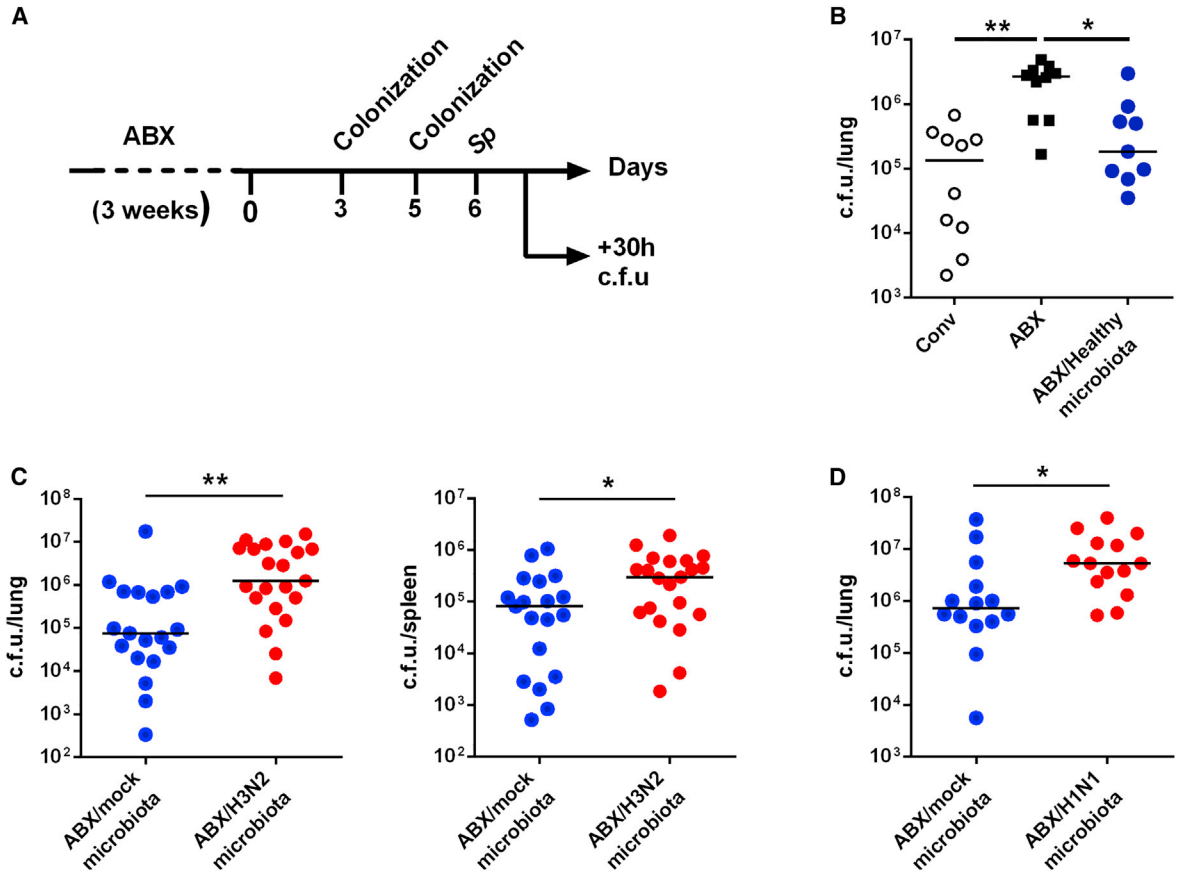

Figure 2. Enhanced Susceptibility to Respiratory Bacterial Infection in Mice Colonized with the IAV-Experienced Microbiota

(A) The experimental design for microbiota adoptive transfer is shown. 1 day after the second colonization, mice were challenged with *S. pneumoniae* (1×10^6 colony-forming units [CFUs]). Non-recolonized ABX-treated mice were infected 3 days after ABX cessation.

(B) The number of viable bacteria in the lung was determined 30 h after the bacterial challenge. The solid lines correspond to the median values (n = 10, pool of two independent experiments).

(C and D) The same procedure was performed, but this time, ABX-treated mice were recolonized with the cecal microbiota collected from mock-treated mice or IAV-infected mice (H3N2 or H1N1, C and D, respectively). n = 19–21 (C) and n = 14 (D) (pool of three or two independent experiments).

Significant differences were determined using the Kruskal-Wallis ANOVA test (B) and the Mann-Whitney U test (C and D) (*$p < 0.05$; **$p < 0.01$).

The IAV-Experienced Microbiota Confers Susceptibility to Respiratory Bacterial Infection

Through the continuous release of soluble factors, the gut microbiota can act at distance to modulate pulmonary immunity (Abt et al., 2012; Bradley et al., 2019; Brown et al., 2017; Clarke et al., 2010; Ichinohe et al., 2011; Schuijt et al., 2016; Steed et al., 2017). We thus investigated the potential consequences of IAV-induced gut dysbiosis on pulmonary antibacterial defenses. To this end, we performed microbiota transfer experiments (experimental protocol in Figure 2A). Using this approach, recent reports have demonstrated that a healthy gut microbiota can enhance resistance to pulmonary pneumococcal infection (serotype 3) (Brown et al., 2017; Clarke et al., 2010; Schuijt et al., 2016). To investigate this putative effect in our experimental model, mice were treated with broad-spectrum antibiotics (ABX), to disrupt the residual microbiota, and were then intranasally challenged with *S. pneumoniae* serotype 1, a major serotype in humans. Relative to conventional (microbiota proficient) mice, ABX-treated mice displayed a greater bacterial load in their lungs, and oral administration of gut microbiota collected from healthy mice restored bacterial clearance (Figure 2B). These data confirm that a transient arrest of microbiota-derived input signals (here due to ABX treatment) can alter the early pulmonary defenses against bacterial infection.

We next determined whether a loss of input signals due to prior influenza infection could compromise antibacterial pulmonary defense. To this end, the gut microbiota collected from IAV-infected mice was transplanted into ABX-treated mice. Strikingly, mice colonized with the IAV (H3N2)-experienced microbiota had a significantly greater bacterial count in the lungs than mice colonized with the mock (control) gut microbiota (Figure 2C, left panel). The dysbiotic IAV-conditioned microbiota also enhanced bacterial dissemination from the lungs, as revealed by the higher number of viable bacteria in the spleen (Figure 2C, right panel). To investigate whether this effect was strain specific, the same procedure was repeated using gut microbiota collected from H1N1-infected mice. This also led to enhanced susceptibility to pulmonary pneumococcal infection (Figure 2D). This finding indicates that the

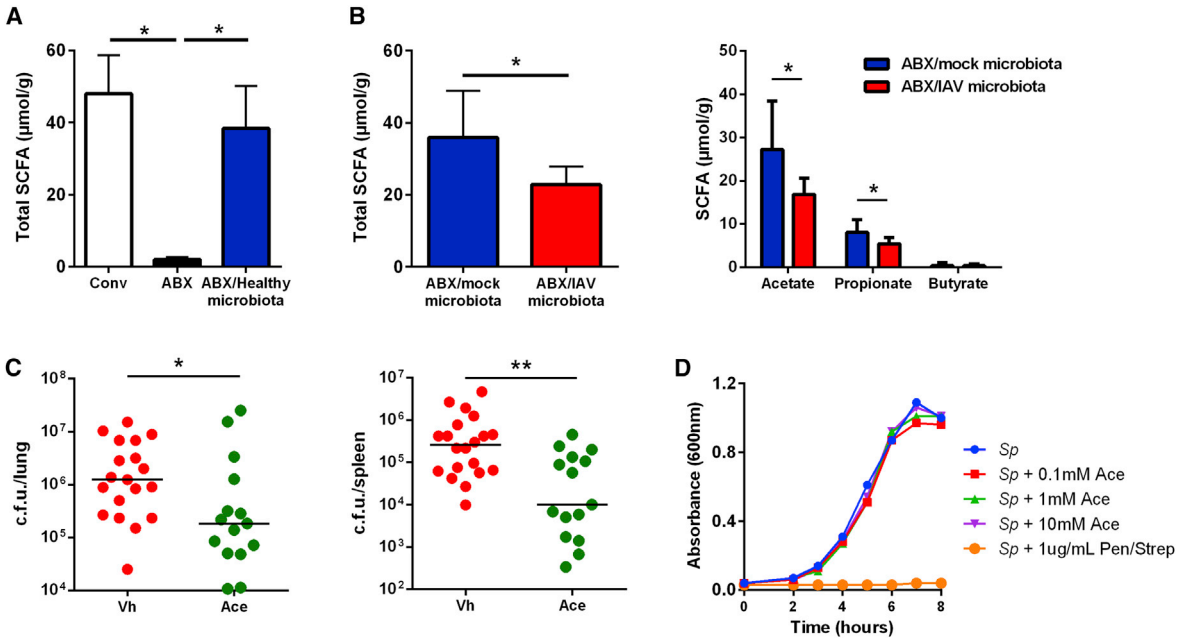

Figure 3. Reduced SCFA Production by the IAV-Experienced Microbiota and Effect of Acetate (Ace) Supplementation on Host Defense against Pneumococcal Infection

(A) Total cecal SCFA concentration in conventional mice, ABX-treated mice, and ABX-treated recolonized mice (n = 4–7, one of two independent experiments shown).

(B) Total (left panel) and individual (right panel) cecal SCFA concentration in mice recolonized with the microbiota collected from mock-treated mice or IAV (H3N2)-infected mice (7 dpi). n = 8 (one of two independent experiments shown).

(C) Recolonized mice (IAV-conditioned microbiota, 7 dpi) were infected with *S. pneumoniae* (1×10^6 CFUs). Mice were treated with Ace (200 mM in drinking water) or vehicle (Vh) 5 days before the pneumococcal challenge (n = 15–20, pool of three independent experiments).

(D) *S. pneumoniae* colonies at exponential growth were added to culture medium in the absence or presence of grading concentrations of Ace or, as a positive control, 1 U/mL penicillin and 1 μg/mL streptomycin. The optical density (O.D.). was measured over time, as stated in the figure.

Results are expressed as the mean ± SD (A and B). Significant differences were determined using the Kruskal-Wallis ANOVA test (A) and the Mann-Whitney U test (B and C) (*$p < 0.05$; **$p < 0.01$).

altered pulmonary response transferred by the IAV-conditioned microbiota is a general consequence of influenza infection, regardless of the viral subtype. Hence, disturbance of the microbial equilibrium in the gut during influenza infection enhances susceptibility to respiratory bacterial infections.

Reduced Acetate Production by the IAV-Experienced Microbiota Is Responsible for Enhanced Susceptibility to Respiratory Bacterial Infections

We next investigated whether the greater susceptibility of mice colonized with the dysbiotic IAV-conditioned microbiota associates with lower SCFA production. As expected, the cecal SCFA concentration was much lower in ABX-treated mice than in conventional animals, and colonization with a healthy microbiota partially restored the SCFA content (Figure 3A). Interestingly, relative to mice colonized with the mock-conditioned microbiota, mice colonized with the IAV-conditioned microbiota had significantly lower concentration of SCFAs (Figure 3B, left panel). In particular, the concentration of acetate and propionate was reduced (Figure 3B, right panel). It is noteworthy that at this time point, the concentration of butyrate remained at basal level. Together, altered respiratory defenses of colonized mice (IAV-conditioned microbiota) associate with reduced SCFA production.

We then addressed the hypothesis that the drop of SCFAs may affect the pulmonary response. To this end, we looked at whether SCFA supplementation of IAV-conditioned microbiota-transplanted mice could reverse the dysfunctional pulmonary response against *S. pneumoniae*. We focused on acetate, as it represents the predominant SCFA found systematically (Cait et al., 2018; Macia et al., 2015; Trompette et al., 2014) and Figure 1E). Remarkably, acetate supplementation (drinking water) diminished bacterial count in the lungs and reduced systemic spread of bacteria from the lungs (Figure 3C). SCFAs can exert bactericidal and/or bacteriostatic functions (Coussens et al., 2015; Wang et al., 2014b). As shown in Figure 3D, acetate had no direct effect on *S. pneumoniae* outgrowth *in vitro*. Together, the fermentation product acetate can restore the defective antibacterial pulmonary response conferred by the dysbiotic IAV-conditioned microbiota.

Restricted Food Intake (Mimicking Influenza Disease) Alters the Gut Microbiota and the Pulmonary Defense against Bacterial Infection

Rapid decreased food intake can alter the composition and the metabolic activity of the gut microbiota (Li et al., 2017). We hypothesized that one of the most influential factors that might

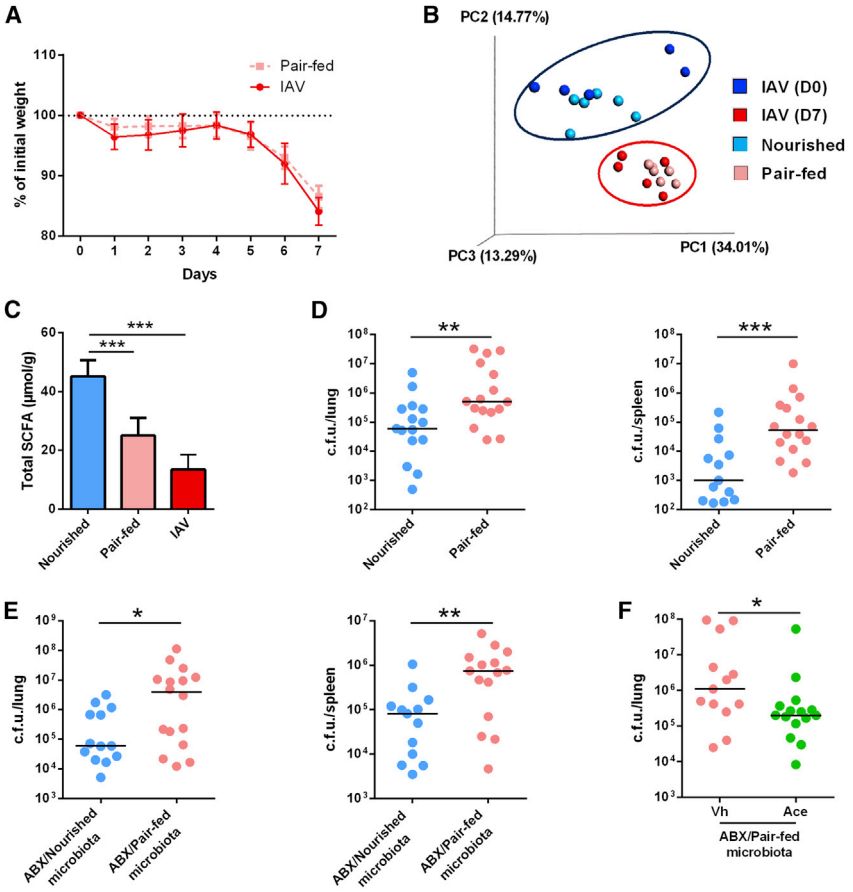

Figure 4. Altered Gut Microbiota and Pulmonary Defense against Pneumococcal Infection in Pair-Fed Mice

(A) Kinetic measurement of body weight loss of pair-fed mice and IAV-infected mice (n = 8, one out of three experiments performed).

(B) Analysis of the gut microbiota (feces) in pair-fed mice. Bacterial diversity following food restriction was determined by PCA and was compared to that in IAV-infected mice (H3N2, 7 dpi).

(C) Concentrations of cecal total SCFAs in nourished mice, pair-fed mice, and IAV-infected (7 dpi) mice (n = 14, pool of two independent experiments).

(D) Nourished and pair-fed mice were infected with *S. pneumoniae* (1×10^6 CFUs).

(E) ABX-treated mice were recolonized with the microbiota collected from nourished mice or from pair-fed mice. Recolonized mice were infected 3 days after the first recolonization (1×10^6 CFUs).

(F) Mice recolonized with the dysbiotic (pair-fed-conditioned) microbiota were treated or not with Ace as described in Figure 3C.

n = 13–16 (D–F) (two pooled experiments). Results are expressed as the mean ± SD (A–C). Significant differences were determined using the Kruskal-Wallis ANOVA test (C) and the Mann-Whitney U test (D–F) (*$p < 0.05$; **$p < 0.01$; ***$p < 0.001$). See also Figure S4 and Table S5.

result in alterations of the gut microbiota during influenza infection is decreased food intake (due to anorexia). In our sublethal infection model, influenza infection is associated with decreased food intake (and body weight loss) from days 4 to 11, with a peak at day 7 (reaching ~85%) (Figure S4A, left panel). In order to test whether gut dysbiosis during influenza infection may be due to reduced food consumption, we designed a pair-feeding experiment. We restricted the food intake of noninfected mice, with reductions of 10%, 35%, and 85% on days 4, 5, and 6, respectively (based on measurement of food consumption by infected animals; Figure S4A, right panel) in order to have body weight loss similar to IAV-infected mice. These pair-fed mice were sacrificed at day 7. As depicted in Figure 4A, pair-fed mice lost weight (relative to normally fed mice) in much the same way as IAV-infected animals and had lost ~15% of their initial weight at the time of the sacrifice. An analysis of the beta diversity clearly showed that the bacterial population from pair-fed mice differed from that of nourished mice and tended to cluster with the population from the IAV-infected mice at 7 dpi (Figure 4B; data not shown). Although the diet-imposed rapid weight loss did not fully recapitulate the phenotype of influenza infection, a taxonomic analysis revealed several common shifts in the diversity and abundance of taxa (e.g., *Parabacteroides*, *Lachnospiraceae*, *Lactobacillus*, *Alphaproteobacteria*, and *Akkermansia*) for pair-fed mice and IAV-infected mice (Figures S4B and S4C; Table S5). Relative to nourished mice, pair-fed mice displayed lower cecal concentration of SCFAs (Figures 4C and S4D).

To investigate the effect of food restriction on the host's pulmonary defenses, pair-fed mice were infected with *S. pneumoniae*. As shown in Figure 4D, the bacterial counts in the lungs and spleen were higher in pair-fed mice than in control mice. To elucidate whether the gut microbiota is causal for this enhanced susceptibility, we performed microbiota transplantation experiments. The experiments indicated that this enhanced susceptibility was at least in part due to altered gut microbiota (Figure 4E). We next tested our presumption that reduced acetate production in pair-fed animals (due to dietary fiber deprivation) could enhance susceptibility to pneumococcal infection. Indeed, acetate supplementation significantly reduced the bacterial load in mice that received the pair-fed-conditioned (dysbiotic) microbiota (Figure 4F). Together, food restriction mimicking influenza disease alters the composition and metabolic activity of the gut microbiota and increases susceptibility to respiratory bacterial infections. These results support the notion that reduced food consumption during influenza infection contributes to dysbiosis and altered pulmonary defenses against bacterial infections.

The IAV-Conditioned Microbiota Impairs the Bactericidal Activity of Alveolar Macrophages, an Effect Restored by Acetate Supplementation

We next sought to gain insights into the mechanisms through which the IAV-conditioned microbiota compromises the host's pulmonary defenses. Alveolar macrophages, conventional

dendritic cells, neutrophils, invariant natural killer T cells (iNKT) cells, and γδ T cells play a (direct or indirect) role in the early clearance of pneumococci (Cao et al., 2014; Nakamatsu et al., 2007; van der Poll and Opal, 2009; Paget and Trottein, 2019). Flow cytometry analysis indicated that colonized mice (mock-conditioned microbiota and IAV-conditioned microbiota) displayed an identical number of these cells in the lungs (Figures 5A, S5A, and S5B). We and others have shown that interferon-γ (IFN-γ) and interleukin-17A (IL-17A) production by iNKT cells and γδ T cells, respectively, contributes to the control of pneumococci outgrowth (Barthelemy et al., 2017; Cao et al., 2014; Hassane et al., 2017). Intracellular flow cytometry indicated a similar number of IFN-γ-expressing iNKT cells and IL-17A-expressing γδ T cells upon *S. pneumoniae* challenge in the two groups of colonized mice (Figure 5B). Phagocytosis is an important early event in the control of *S. pneumoniae*. To evaluate this, colonized mice were infected with EGFP-expressing *S. pneumoniae* (serotype 1), and 4 h later, cells were collected from the bronchoalveolar lavage (BAL) fluids. At this time point, alveolar macrophages represented by far the main cell population in the BAL fluids (>95%), and their numbers were similar in the two groups (data not shown). Confocal microscopy did not reveal any significant differences between the groups of animals with regard to (1) the frequency of macrophages having internalized *S. pneumoniae* and (2) the average number of internalized bacteria per macrophage (Figures 5C and 5D). Quantitative real-time PCR (16S *S. pneumoniae*) assay on sorted alveolar macrophages confirmed this finding (Figure 5E). We next turned to investigate potential alteration of the bactericidal activity of alveolar macrophages. To evaluate this, the killing activity of alveolar macrophages was measured. Compared to the control group, alveolar macrophages collected from IAV-conditioned microbiota-colonized mice displayed an altered capacity to kill pneumococci (Figure 5F). Indeed, in this animal group, an enhanced number of viable internalized bacteria were counted after macrophage lysis and bacterial culture. Hence, alveolar macrophages (IAV-conditioned microbiota) kill pneumococci less effectively.

We then looked at whether acetate treatment of colonized mice (IAV-conditioned microbiota) could affect pulmonary cell number and/or activation. Relative to controls, acetate treatment did not significantly modify the frequency/number of macrophages, conventional dendritic cells, neutrophils, and unconventional T cells or the activation threshold of the later (Figures 5A, 5B, and S5B). We then investigated whether acetate treatment could reverse the altered effector functions of alveolar macrophages. Acetate treatment had no impact on phagocytosis activity of alveolar macrophages but enhanced their killing activity (Figures 5D–5F). To further demonstrate the role of alveolar macrophages in acetate-induced pulmonary defense, colonized mice were treated with clodronate-loaded liposomes. Macrophage depletion (Figure S5C) abrogated the protective effect of acetate (Figure 5G). To investigate whether acetate directly targets macrophages, killing assays were performed *in vitro*. Pretreatment of macrophages with acetate enhanced the killing of pneumococci (Figure 5H). Collectively, the dysbiotic IAV-conditioned microbiota lowers pneumococci clearance through impairment of alveolar macrophage functions, an effect restored by acetate supplementation.

Supplementation of Acetate during Influenza Protects against Lethal Bacterial Superinfection

We then investigated the potential contribution of altered SCFA production during IAV infection on secondary bacterial infection. To this end, IAV-infected mice were treated with acetate and secondarily infected with *S. pneumoniae* at day 7, the peak of susceptibility. Remarkably, acetate supplementation lowered the bacterial load in the lungs and resulted in reduced systemic spread of bacteria from the lungs in double-infected mice (Figure 6A). The combined use of acetate, propionate and butyrate did not further enhance resistance, relative to acetate alone (Figure S6A). Of note, the protective effect triggered by acetate did not associate with major changes in the composition of the gut microbiota (Figures 6B, S6B, and S6C). To determine the effect of acetate on pulmonary damage, we evaluated and scored lung samples histopathologically. Compared to the control group, acetate-treated mice had less marked pneumonia, including perivascular inflammatory infiltrates (Figure 6C). We then determined whether the positive effect of acetate on bacterial loads and lung pathology extended to ameliorated morbidity and mortality outcomes. While acetate treatment had no effect on weight loss due to IAV infection, it favored weight regain after secondary pneumococcal infection (Figure S7A). Most notably, supplementation of acetate during the course of IAV infection effectively and significantly improved survival of double-infected mice (~50% survival rate; Figure 6D).

We next assessed mechanisms through which acetate was able to ameliorate disease outcomes of superinfected mice. Virus-induced alteration of epithelial barrier functions contributes to bacterial superinfection (Barthelemy et al., 2018; McCullers, 2014; Rynda-Apple et al., 2015). Acetate treatment did not affect viral load in lungs and had no effect on the expression of genes associated with pulmonary barrier functions, the expression of which was strongly altered during influenza (Figure 6E). Likewise, acetate failed to affect the expression of IFN-inducible genes and antiviral mediators (Figure S7B). Hence, acetate does not act on viral replication and associated epithelial dysfunction. We then reasoned that the beneficial effect of acetate might rely on antibacterial functions of immune cells. Compared to controls, acetate treatment did not modify the number of macrophages, conventional dendritic cells, neutrophils, IFN-γ-expressing iNKT cells, and IL-17A-expressing γδ T cells (Figures S7C and S7D). Of interest, macrophage depletion by clodronate-liposome inoculation abrogated the beneficial effect of acetate (Figure 6F). Taken as a whole, low acetate production during influenza infection influences susceptibility to secondary bacterial infection, and supplementation of acetate (in part through macrophages) is sufficient to improve disease outcomes.

Exogenous Administration of a Synthetic FFAR2 Agonist Protects against Post-influenza Secondary Bacterial Infection

Acetate can act through the G-protein-coupled receptors FFAR2 (formerly GPR43) and, to a lesser extent, FFAR3 (formerly GPR41) (Milligan et al., 2017). Relative to FFAR2-competent mice, acetate failed to significantly lower bacterial loads in superinfected *Ffar2*$^{-/-}$ mice (Figure 7A). Of note, no significant difference was noticed in terms of viral (not shown) and bacterial loads between

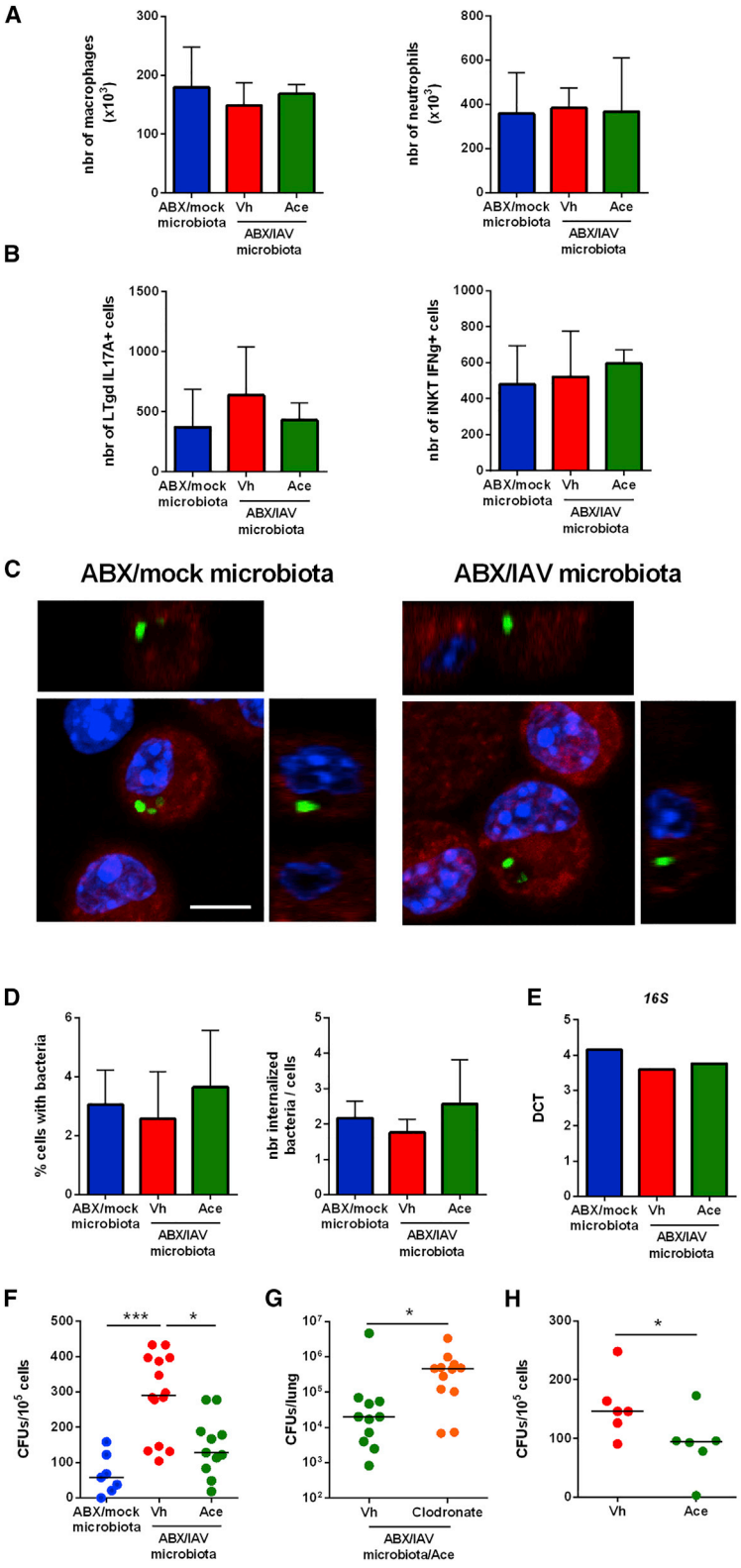

Figure 5. Altered Bactericidal Activity of Alveolar Macrophages in Mice Recolonized with the Dysbiotic IAV Microbiota

(A) Lung cells from recolonized mice were analyzed by flow cytometry. The mean number ± SD of alveolar macrophages and neutrophils are depicted.

(B) Recolonized mice were infected with *S. pneumoniae* (1×10^6 CFUs), and 16 h later, the mean number ± SD of iNKT cells positive for IFN-γ and $\gamma\delta$ T cells positive for IL-17A were determined. n = 8 (A and B) (two pooled experiments).

(C) Colonized mice were infected with EGFP-expressing *S. pneumoniae* (1×10^6 CFUs). 4 h later, binding and internalization of bacteria (green) was assessed by confocal microscopy. Representative images are shown. Nuclei (blue) were visualized by staining with DAPI. The central image is a maximum intensity projection of the image stack (scale bars, 10 μm; insert magnification, 2×). Top and right: orthogonal view for the axis yz and xz.

(D) The frequency of macrophages having internalized *S. pneumoniae* and the average number of internalized bacteria per macrophage are depicted (n = 6; one representative experiment out of two).

(E) Quantification of *S. pneumoniae* in sorted alveolar macrophages (4 h after infection) by quantitative PCR. Data were normalized against expression of the *gapdh* gene, and data are expressed as ΔCt. One representative experiment out of two is depicted.

(F) Alveolar macrophages were collected from colonized mice 4 h after *S. pneumoniae* infection. After extensive washing, cells were lysed and plated on blood agar plates. The number of viable bacteria is expressed per 1×10^5 cells (n = 7–14, two pooled experiments).

(G) Ace-treated colonized mice (ABX/IAV) were treated with clodronate-loaded liposomes or empty liposomes 16 h before *S. pneumoniae* challenge (intranasal route) (n = 11–12, two pooled experiments).

(H) Macrophages were pretreated with Ace (10 mM) for 1 h and next exposed to opsonized *S. pneumoniae*. The number of viable bacteria was assessed 2 h post-bacterial exposure by counting CFUs from cellular lysate. Data are representative of two independent experiments (n = 6).

Results are expressed as the mean ± SD (A, B, and D). Significant differences were determined using the Kruskal-Wallis ANOVA test (A, B, and D–F) and the Mann-Whitney U test (G and H) (*$p < 0.05$; **$p < 0.01$; ***$p < 0.001$). See also Figure S5.

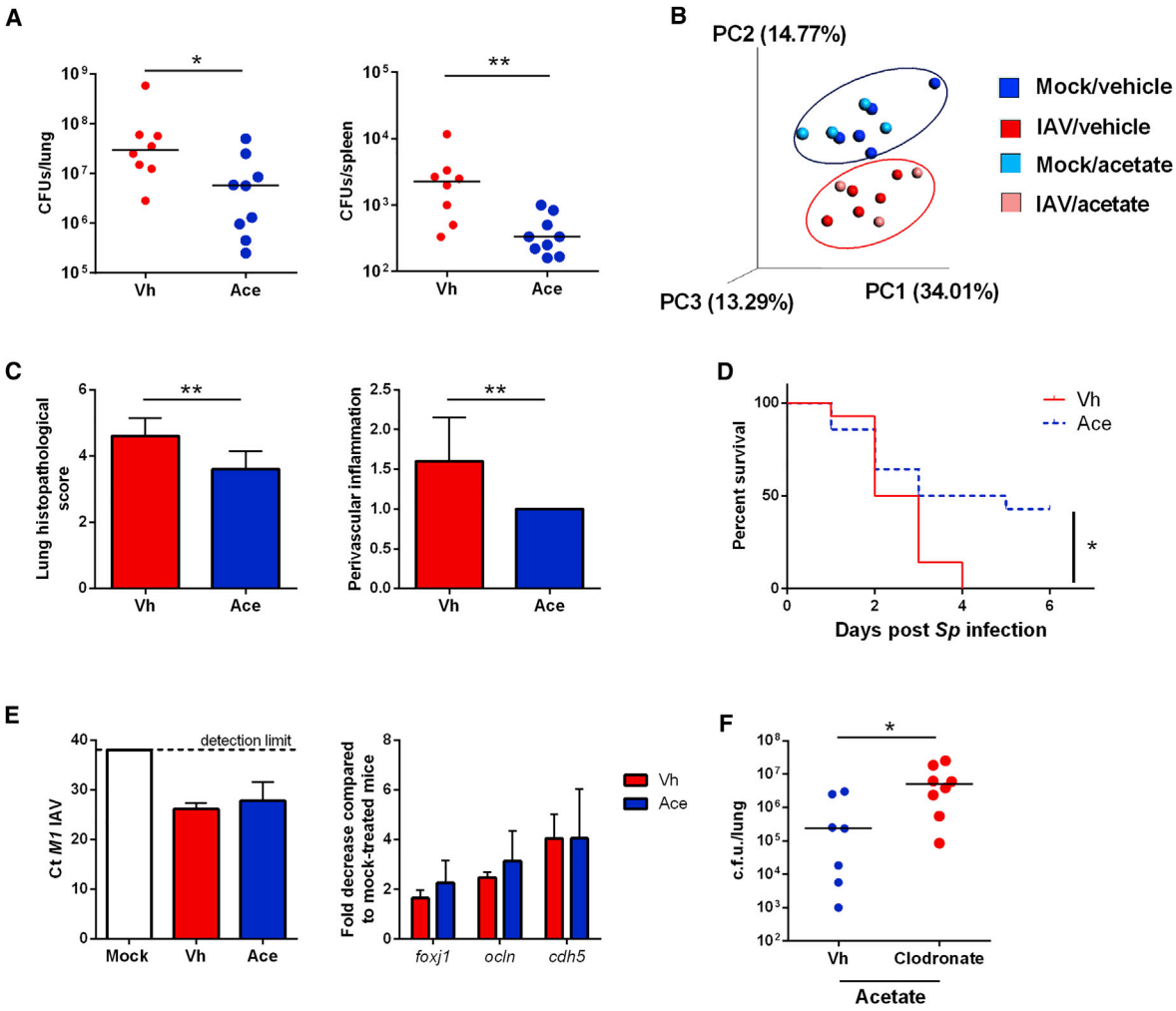

Figure 6. Effect of Ace Supplementation in Mice Doubly Infected with IAV and *S. pneumoniae*

IAV-infected mice were treated with Ace (200 mM in drinking water) or Vh at 2 dpi, 5 days before the pneumococcal challenge (1×10^3 CFUs).

(A) The number of bacteria was determined 30 h after the *S. pneumoniae* challenge (n = 8–9, one representative experiment out of four is shown).

(B) PCA was performed on samples (cecum) collected from uninfected mice treated (bright blue) or not (dark blue) with Ace for 5 days and from mice infected 7 days earlier with H1N1 and treated (pink) or not (red) with Ace at 2 dpi (n = 4–5).

(C) Histological analysis of lung sections. Blinded sections were scored for levels of pneumonia (left; sum of different parameters), including perivascular inflammatory infiltrates (right) (n = 4 mice/group).

(D) The survival of superinfected animals was monitored (n = 14, two pooled experiments).

(E) Left: IAV *M1* mRNA levels were measured in the whole lungs by quantitative RT-PCR. Data are expressed as Ct values. The dashed line represents the detection threshold. Right: mRNA copy numbers of genes were quantified by RT-PCR. Data are expressed as fold increase over average gene expression in mock-treated animals. One representative experiment out of two is shown (n = 5). *Cdh5*, VE-cadherin; *Ocln*, occluding).

(F) Ace-treated IAV-infected mice were depleted (clodronate containing liposomes), or not (empty liposomes), in alveolar macrophages before the pneumococcal challenge (n = 7–8, one experiment performed).

Results are expressed as the mean ± SD (C and E). Significant differences were determined using the Mann-Whitney U test (A and F) or ANOVA followed by the Holm-Sidak test (C). In (D), survival of mice was compared using Kaplan-Meier analysis and the log-rank test (*$p < 0.05$; **$p < 0.01$). See also Figures S6 and S7.

vehicle-treated wild-type and *Ffar2*$^{-/-}$ mice. FFAR2 is amenable to pharmacological manipulation *in vivo* (Milligan et al., 2017). Of note, alveolar macrophages expressed transcripts for *ffar2*, while *ffar3* mRNA expression was much lower (16-fold less expression) (Figure 7B). To investigate the potential consequences of local FFAR2 activation on post-influenza bacterial superinfection, mice were treated with TUG-1375 (a selective FFAR2 agonist) by intra-nasal administration. Pharmacological FFAR2 activation, just before pneumococcal challenge, led to a significant reduction of lung bacterial burden and dissemination to blood (Figure 7C). In contrast, the selective FFAR3 agonist AR420626 failed to confer any protection (Figure 7D). Hence, the FFAR2 agonist TUG-1375 provided the same benefit as acetate in the treatment of post-influenza bacterial superinfection. This latter finding opens up important new possibilities for pharmacological management of post-influenza bacterial superinfection.

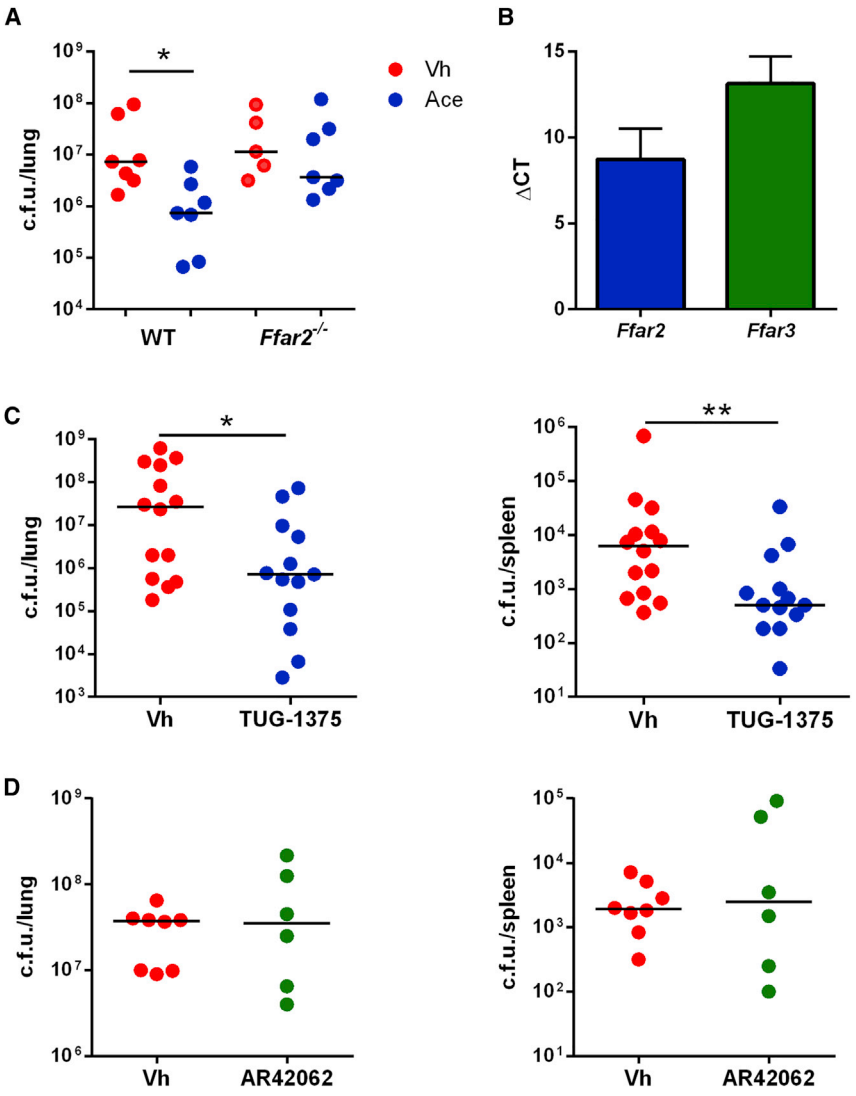

Figure 7. Effect of FFAR2 Agonist Treatment on Bacterial Superinfection Post-influenza

(A) Wild-type (WT) mice and *Ffar2*$^{-/-}$ mice (littermates) were treated with Ace as in Figure 6A (n = 5–7, one representative experiment out of two is shown).

(B) *Ffar2* and *Ffar3* transcript levels were assessed by quantitative RT-PCR on enriched alveolar macrophages (two independent experiments).

(C and D) IAV-infected mice were treated with the selective FFAR2 agonist TUG-1375 (C) or with the selective FFAR3 agonist AR420626 (D) (1 mM in 50 μL, intranasal [i.n.] route) or Vh 16 h before the pneumococcal challenge. n = 13–14 (C) (two pooled experiments) and n = 6–8 (D) (one representative experiment out of two).

Results are expressed as the mean ± SD. Significant differences were determined using the Kruskal-Wallis ANOVA test (A) and the Mann-Whitney U test (B–D) (*p < 0.05; **p < 0.01).

DISCUSSION

A large body of research indicates that alterations in the gut microbiota have a role in the pathogenesis of various chronic diseases. The present study sought to analyze the impact of an acute respiratory infection on the gut microbiota and study the consequences of any functional perturbations on disease outcomes. Our results showed that influenza infection alters the composition and functionality of the gut microbiota and that these changes account for enhanced susceptibility to secondary pulmonary bacterial infections. Our study also highlighted the importance of gut-microbiota-derived SCFAs (acetate) on the host's pulmonary defenses against bacterial (super)infections.

Recent reports have indicated that influenza infections in humans (H7N9) and in murine models (H1N1 and H5N1) alter the composition of the gut microbiota (Bartley et al., 2017; Deriu et al., 2016; Groves et al., 2018; Qin et al., 2015; Wang et al., 2014a; Yildiz et al., 2018). Our data confirm and extend these findings (both H3N2 and H1N1 subtypes). In our settings (sublethal inocula), influenza infection altered the relative abundances of microbial taxa at 7 dpi in both the cecum and the colon, resulting in significant changes in beta diversity. In contrast to chronic diseases in which phylogenic diversity falls markedly, we observed marked changes for lower taxonomic affiliations during influenza. At 7 dpi, we observed the emergence of several bacterial genera that were absent or almost absent in noninfected animals, notably *Escherichia* (Proteobacteria) and the mucus-degrading bacterium *Akkermansia* (Verrucomicrobia). Importantly, the alteration of the gut microbiota's composition at 7 dpi was associated with a concomitant drop in the intestinal concentration of SCFAs, an effect that might have been due to lower abundances of SCFA-producing bacteria. Among potential candidates (with low numbers at 7 dpi; see Tables S2 and S4) are *Lachnospiraceae* (Firmicutes), *Lactobacillaceae (lactobacillus* genus), and *Bifidobacteriaceae* (Actinobacteria) families, which are notable for containing many species capable of fermenting complex carbohydrates into SCFAs. In line with the known resilience of the gut community to short-term perturbations, the microbiota changes during influenza infection were transient with an overall return to a baseline profile at 14 dpi. At this time point, mice recover from weight loss and display higher resistance to secondary bacterial infections (Barthelemy et al., 2016; data not shown).

Food intake and diet composition can rapidly shape the structure and function of the gut microbiota (David et al., 2014; Desai et al., 2016; Maslowski et al., 2009). Moreover, previous studies have revealed that fasting and feeding rhythms significantly alter the gut microbiota (Thaiss et al., 2016). Loss of appetite is a

feature of influenza (Monto et al., 2000). In view of our present results, we suggest that decreased food intake during influenza infection, and thus reduced amounts of ingested complex carbohydrates, from 4 dpi onward is at least partly responsible for perturbation of the microbiota. Indeed, food-restricted mice (mimicking the situation in influenza) displayed several microbiota changes also found in IAV-infected mice, including, for instance, *Lachnospiraceae* and *Lactobacillus* (reduced) and *Alphaproteobacteria* and *Akkermansia* (augmented). As also observed during influenza infection, food restriction was associated with a drop in SCFA production. Reduced availability of dietary fibers and complex carbohydrates due to food restriction may influence competition between gut commensals at the expense of SCFA producers and to the benefit of bacteria using host mucins as an energy source (Desai et al., 2016). Acute starvation in mice decreases host resistance to respiratory pneumococcal infection (Mancuso et al., 2006). In our model of pair-feeding that mimicked the situation encountered during IAV infection, we observed increased susceptibility to *S. pneumoniae*. Fecal transfer experiments indicated that perturbation of the gut microbiota of pair-fed mice has an impact on pulmonary defenses, an effect reversed by supplementation of the fermentation product acetate. This raises important questions about the consequences of severely reduced food (fiber) intake (e.g., due to pathologies, stresses, or voluntary fasting) on the delivery of immune regulatory signals by the gut microbiota, a topic that warrants further investigation. Although we cannot completely rule out the existence of other mechanisms, including systemic or local inflammatory factors (such as IFNs) (Deriu et al., 2016; Wang et al., 2014a), our data argue strongly for a critical role of altered nutritional status (due to anorexia) in dysregulation of the microbiota's composition and function during influenza infection. The reduced consumption of fruit and vegetables rich in fibers (an indirect source of SCFAs) in western countries, and the associated reduced richness of the gut microbiota, is likely to amplify this phenomenon.

Recent data indicate that dysbiosis in the upper respiratory compartment contributes to post-influenza secondary bacterial infections (Planet et al., 2016). The present study is the first to have addressed the question of whether alterations in the gut microbiota might predispose to secondary bacterial infections of the lung. A continuous input from complex microbiota is necessary to maintain the (pulmonary) innate immune system. We hypothesized that a loss of input from gut-microbiota-derived signals during IAV infection may have negative consequences on pulmonary defenses against bacterial infection. Fecal transfer experiments demonstrated that (metabolic) gut microbiota changes during influenza infection have an impact on respiratory bacterial infection (enhanced local outgrowth and dissemination from the lungs). Our data are in line with recent reports demonstrating that a healthy gut microbiota favors pulmonary host defense by improving the antibacterial activities of alveolar macrophages (Brown et al., 2017; Clarke, 2014; Lankelma et al., 2017; Schuijt et al., 2016). These cells are particularly relevant in bacterial infections, since loss of their functions (e.g., during influenza) favors the replication of opportunistic pathogenic bacteria, including *S. pneumoniae* (Ghoneim et al., 2013; Sun and Metzger, 2014). Of interest, while supplementation of NOD-like receptor agonists is sufficient to restore pulmonary defense in microbiota-depleted (ABX) mice (Brown et al., 2017), our study indicates that in IAV microbiota-colonized mice, supplementation with acetate is sufficient to restore host defense against *S. pneumoniae*. However, we cannot exclude that in addition to reduced SCFA (acetate), the dysbiotic IAV gut microbiota might suppress antibacterial defense in the lungs via other mechanisms yet to be unraveled. It is noteworthy that both NOD-like receptor agonists (Brown et al., 2017) and acetate (the present study) converge on enhanced macrophage effector functions (bactericidal activity). Hence, the gut SCFA acetate can target alveolar macrophages, a pathway affected during IAV infection. It is likely that acetate directly targets alveolar macrophages. Our recent data showed that IAV infection affects monopoiesis in the bone marrow (Beshara et al., 2018), a phenomenon not perturbed by exogenous acetate treatment (not shown). Our results agree with a report demonstrating that gut SCFAs can distally target macrophages (microglia, the brain's resident macrophages) to promote their innate effector functions (Erny et al., 2015). They are also in agreement with Galvão and collaborators, who showed that acetate protects against *Klebsiella pneumoniae* (a Gram-negative bacterium) respiratory infection, an effect that depended on FFAR2 (Galvão et al., 2018).

Our findings are in line with the emerging concept whereby gut SCFAs remotely influence immune responses in the lungs and can modulate disease outcomes, including asthmatic reactions (Cait et al., 2018; Maslowski et al., 2009; Trompette et al., 2014) and respiratory viral and bacterial infections (Antunes et al., 2019; Chakraborty et al., 2017; Galvão et al., 2018; Moriyama and Ichinohe, 2019; Trompette et al., 2018). The SCFAs' potential role in innate immune defenses against respiratory infections has yet to be characterized in detail. Importantly, acetate supplementation reduced, in a FFAR2-dependent manner, the bacterial burden after the episode of influenza, despite the immunosuppressive environment imposed by IAV. Of importance, this translated into reduced lung pathology and improved survival rate of double-infected mice. Manipulation of the gut microbiota (which, as we show, becomes deleterious during influenza) might represent an interesting option to limit post-influenza bacterial superinfections. Importantly, Trompette and collaborators have demonstrated that preventive supplementation of diets enriched in fibers protected against influenza infection (lower virus load and pathology) (Trompette et al., 2018). This treatment is associated with enhanced frequency of *Bifidobacterium* and *Bacteroides* genus and enhanced levels of SCFAs (particularly butyrate). Remarkably, butyrate controls influenza infection by reducing, through enhanced $CD8^+$ T cell activity, viral replication. This report is fully in line with our current study, although the consequences of high-fiber diets (or acetate-yielding diets) on secondary bacterial infections are presently unknown. Preventive consumption of fermentable fibers, by protecting the SCFA-producing compartment, may maintain intestinal homeostasis and reinforce the lung's defenses (against IAV and bacteria) during influenza. In the same line, probiotics (e.g., SCFA producers such as the Bifidobacteria and *Lactobacillus* spp) have been successfully used in the context of IAV infection (Zelaya et al., 2016), although their impact on superinfection was not

characterized. In the future, strategies that seek to harness the power of the gut microbiota (via pre-/probiotics) to manage influenza infections might help to control both viral diseases and the harmful viral/bacterial synergy during bacterial superinfections. Alternatively, the use of SCFAs or FFAR2 agonists as therapeutics might be envisaged to lower bacterial superinfection post-influenza. FFAR2 agonists are viewed as a promising treatment of metabolic syndromes such as type 2 diabetes and obesity (Milligan et al., 2017; Ulven, 2012). Our study shows the positive effect of a synthetic FFAR2 agonist in respiratory infection and highlights a new opportunity for further development against bacterial pneumonia.

The present study provided evidence that during influenza infection, extrapulmonary disorders, namely dysbiosis, can negatively influence bacterial superinfection. Further research in this direction might help to define predictive markers (i.e., systemic SCFAs) and/or develop therapeutic approaches against these superinfections. Lastly, our findings might have broader applications in the treatment of acute diseases associated with an altered microbiota and secondary infections such as trauma, burns, and sepsis.

STAR★METHODS

Detailed methods are provided in the online version of this paper and include the following:

- KEY RESOURCES TABLE
- LEAD CONTACT AND MATERIALS AVAILABILITY
- EXPERIMENTAL MODEL AND SUBJECT DETAILS
  - Mice and ethics statement
  - Viruses and bacteria
- METHOD DETAILS
  - Diets
  - Infections and assessment of bacterial loads
  - Reagents, antibodies, flow cytometry and cell sorting
  - Sample collection, DNA extraction and 16S rRNA gene copy number
  - 16S rRNA gene pyrosequencing and data processing
  - Taxonomic Affiliation and diversity analyses
  - Measurement of food consumption and pair-feeding experiments
  - Measurement of SCFA concentrations and treatment with acetate or FFAR2/FFAR3 agonists
  - Quantification of viral loads and assessment of gene expression by quantitative RT-PCR
  - Microbiota transfer experiments
  - *In vivo* phagocytosis and killing assays and assessment of pneumococcal load in alveolar macrophages
  - *In vitro* killing assay
  - S. pneumoniae outgrowth *in vitro*
- QUANTIFICATION AND STATISTICAL ANALYSIS
- DATA AND CODE AVAILABILITY

SUPPLEMENTAL INFORMATION

Supplemental Information can be found online at https://doi.org/10.1016/j.celrep.2020.02.013.

ACKNOWLEDGMENTS

This work is dedicated to the memory of Professor André Capron (1930–2020).

This work was supported in part by INSERM, CNRS, University of Lille, Pasteur Institute of Lille, région des Hauts-de-France, state of Minais Gerais/FAPEMIG (Franco-Brazilian call 2014-2015, FLUMICROBIOT, to F.T. and M.T.), Innovation Fund Denmark (grant 0603-00452B to T.U.), the Biotechnology and Biosciences Research Council (grant BB/S000453/1 to G.M.), and Agence Nationale de la Recherche (grant ANR-17-CE15-0020-01, ACROBAT, to F.T.). V.S. and A.B. received salary support (PhD fellowship) from Lille University and the Fondation pour la Recherche Médicale (V.S.). Dr. J.W. Veening (University of Groningen, the Netherlands) is acknowledged for the gift of the EGFP-expressing bacteria and Dr. D.H. Dockrell and G. Marshall (Sheffield, UK) for their advice on killing assays. We thank Dr. A. Højgaard Hansen for assistance with compound synthesis. We acknowledge the generous support from the NIAID Tetramer Facility (Emory University, Atlanta, GA) for supplying CD1d tetramers. We also thank the BICeL flow cytometry core facility for technical assistance and the animal facility of the Pasteur Institute, Lille.

AUTHOR CONTRIBUTIONS

F.T. conceived and supervised this study. A.T.V., B.F., C.P., I.W., C.F., R.L.G., M.T., S.F., M.M.T., and F.T. designed the experiments. V.S., A.B., L.P.T., and M.G.M. performed most of the experiments. M.L.N. and C.C. conducted SCFA quantification. C.M.Q.-J. scored lung histology slides. V.S. and D.S. conducted flow cytometry and killing assay. S.S.-D. performed the confocal analysis. S.F. conducted statistical analysis (16S sequencing). G.M. and T.U. provided FFAR2 and FFAR3 synthetic ligands and insights into their use. G.M. provided *Ffar2*$^{-/-}$ mice. V.S., A.B., L.P.T., M.G.M., S.F., M.M.T., and F.T. analyzed the data. F.T. wrote the manuscript, with input from all authors.

DECLARATION OF INTERESTS

A.B., V.S., M.M.T., L.P.T., F.T., and A.T.V. are inventors of patent WO2019149727, "Use of short chain fatty acids for the treatment of bacterial superinfections post-influenza." V.S., T.U., and F.T. are inventors of patent EP19188615.9, "Use of free fatty acid receptor 2 agonists for the treatment of bacterial superinfections post-influenza."

Received: September 24, 2019
Revised: December 13, 2019
Accepted: February 4, 2020
Published: March 3, 2020

REFERENCES

Abt, M.C., Osborne, L.C., Monticelli, L.A., Doering, T.A., Alenghat, T., Sonnenberg, G.F., Paley, M.A., Antenus, M., Williams, K.L., Erikson, J., et al. (2012). Commensal bacteria calibrate the activation threshold of innate antiviral immunity. Immunity *37*, 158–170.

Antunes, K.H., Fachi, J.L., de Paula, R., da Silva, E.F., Pral, L.P., Dos Santos, A.Á., Dias, G.B.M., Vargas, J.E., Puga, R., Mayer, F.Q., et al. (2019). Microbiota-derived acetate protects against respiratory syncytial virus infection through a GPR43-type 1 interferon response. Nat. Commun. *10*, 3273.

Arpaia, N., Campbell, C., Fan, X., Dikiy, S., van der Veeken, J., deRoos, P., Liu, H., Cross, J.R., Pfeffer, K., Coffer, P.J., and Rudensky, A.Y. (2013). Metabolites produced by commensal bacteria promote peripheral regulatory T-cell generation. Nature *504*, 451–455.

Ballinger, M.N., and Standiford, T.J. (2010). Postinfluenza bacterial pneumonia: host defenses gone awry. J. Interferon Cytokine Res. *30*, 643–652.

Barthelemy, A., Ivanov, S., Hassane, M., Fontaine, J., Heurtault, B., Frisch, B., Faveeuw, C., Paget, C., and Trottein, F. (2016). Exogenous activation of invariant natural killer T cells by α-galactosylceramide reduces pneumococcal outgrowth and dissemination postinfluenza. mBio *7*, e01440-16.

Barthelemy, A., Ivanov, S., Fontaine, J., Soulard, D., Bouabe, H., Paget, C., Faveeuw, C., and Trottein, F. (2017). Influenza A virus-induced release of

interleukin-10 inhibits the anti-microbial activities of invariant natural killer T cells during invasive pneumococcal superinfection. Mucosal Immunol. *10*, 460–469.

Barthelemy, A., Sencio, V., Soulard, D., Deruyter, L., Faveeuw, C., Le Goffic, R., and Trottein, F. (2018). Interleukin-22 immunotherapy during severe influenza enhances lung tissue integrity and reduces secondary bacterial systemic invasion. Infect. Immun. *86*, e00706-17.

Bartley, J.M., Zhou, X., Kuchel, G.A., Weinstock, G.M., and Haynes, L. (2017). Impact of age, caloric restriction, and influenza infection on mouse gut microbiome: an exploratory study of the role of age-related microbiome changes on influenza responses. Front. Immunol. *8*, 1164.

Beshara, R., Sencio, V., Soulard, D., Barthélémy, A., Fontaine, J., Pinteau, T., Deruyter, L., Ismail, M.B., Paget, C., Sirard, J.-C., et al. (2018). Alteration of Flt3-Ligand-dependent de novo generation of conventional dendritic cells during influenza infection contributes to respiratory bacterial superinfection. PLoS Pathog. *14*, e1007360.

Blander, J.M., Longman, R.S., Iliev, I.D., Sonnenberg, G.F., and Artis, D. (2017). Regulation of inflammation by microbiota interactions with the host. Nat. Immunol. *18*, 851–860.

Bradley, K.C., Finsterbusch, K., Schnepf, D., Crotta, S., Llorian, M., Davidson, S., Fuchs, S.Y., Staeheli, P., and Wack, A. (2019). Microbiota-driven tonic interferon signals in lung stromal cells protect from influenza virus infection. Cell Rep. *28*, 245–256.e4.

Brown, R.L., Sequeira, R.P., and Clarke, T.B. (2017). The microbiota protects against respiratory infection via GM-CSF signaling. Nat. Commun. *8*, 1512.

Budden, K.F., Gellatly, S.L., Wood, D.L.A., Cooper, M.A., Morrison, M., Hugenholtz, P., and Hansbro, P.M. (2017). Emerging pathogenic links between microbiota and the gut-lung axis. Nat. Rev. Microbiol. *15*, 55–63.

Cait, A., Hughes, M.R., Antignano, F., Cait, J., Dimitriu, P.A., Maas, K.R., Reynolds, L.A., Hacker, L., Mohr, J., Finlay, B.B., et al. (2018). Microbiome-driven allergic lung inflammation is ameliorated by short-chain fatty acids. Mucosal Immunol. *11*, 785–795.

Cao, J., Wang, D., Xu, F., Gong, Y., Wang, H., Song, Z., Li, D., Zhang, H., Li, D., Zhang, L., et al. (2014). Activation of IL-27 signalling promotes development of postinfluenza pneumococcal pneumonia. EMBO Mol. Med. *6*, 120–140.

Chakraborty, K., Raundhal, M., Chen, B.B., Morse, C., Tyurina, Y.Y., Khare, A., Oriss, T.B., Huff, R., Lee, J.S., St Croix, C.M., et al. (2017). The mito-DAMP cardiolipin blocks IL-10 production causing persistent inflammation during bacterial pneumonia. Nat. Commun. *8*, 13944.

Clarke, T.B. (2014). Microbial programming of systemic innate immunity and resistance to infection. PLoS Pathog. *10*, e1004506.

Clarke, T.B., Davis, K.M., Lysenko, E.S., Zhou, A.Y., Yu, Y., and Weiser, J.N. (2010). Recognition of peptidoglycan from the microbiota by Nod1 enhances systemic innate immunity. Nat. Med. *16*, 228–231.

Coussens, A.K., Wilkinson, R.J., and Martineau, A.R. (2015). Phenylbutyrate is bacteriostatic against Mycobacterium tuberculosis and regulates the macrophage response to infection, synergistically with 25-hydroxy-vitamin D3. PLoS Pathog. *11*, e1005007.

David, L.A., Maurice, C.F., Carmody, R.N., Gootenberg, D.B., Button, J.E., Wolfe, B.E., Ling, A.V., Devlin, A.S., Varma, Y., Fischbach, M.A., et al. (2014). Diet rapidly and reproducibly alters the human gut microbiome. Nature *505*, 559–563.

De Weirdt, R., Possemiers, S., Vermeulen, G., Moerdijk-Poortvliet, T.C.W., Boschker, H.T.S., Verstraete, W., and Van de Wiele, T. (2010). Human faecal microbiota display variable patterns of glycerol metabolism. FEMS Microbiol. Ecol. *74*, 601–611.

Deriu, E., Boxx, G.M., He, X., Pan, C., Benavidez, S.D., Cen, L., Rozengurt, N., Shi, W., and Cheng, G. (2016). Influenza virus affects intestinal microbiota and secondary Salmonella infection in the gut through type I interferons. PLoS Pathog. *12*, e1005572.

Desai, M.S., Seekatz, A.M., Koropatkin, N.M., Kamada, N., Hickey, C.A., Wolter, M., Pudlo, N.A., Kitamoto, S., Terrapon, N., Muller, A., et al. (2016). A dietary fiber-deprived gut microbiota degrades the colonic mucus barrier and enhances pathogen susceptibility. Cell *167*, 1339–1353.e21.

Erny, D., Hrabě de Angelis, A.L., Jaitin, D., Wieghofer, P., Staszewski, O., David, E., Keren-Shaul, H., Mahlakoiv, T., Jakobshagen, K., Buch, T., et al. (2015). Host microbiota constantly control maturation and function of microglia in the CNS. Nat. Neurosci. *18*, 965–977.

Galvão, I., Tavares, L.P., Corrêa, R.O., Fachi, J.L., Rocha, V.M., Rungue, M., Garcia, C.C., Cassali, G., Ferreira, C.M., Martins, F.S., et al. (2018). The metabolic sensor GPR43 receptor plays a role in the control of *Klebsiella pneumoniae* infection in the lung. Front. Immunol. *9*, 142.

Ghoneim, H.E., Thomas, P.G., and McCullers, J.A. (2013). Depletion of alveolar macrophages during influenza infection facilitates bacterial superinfections. J. Immunol. *191*, 1250–1259.

Groves, H.T., Cuthbertson, L., James, P., Moffatt, M.F., Cox, M.J., and Tregoning, J.S. (2018). Respiratory disease following viral lung infection alters the murine gut microbiota. Front. Immunol. *9*, 182.

Hansen, A.H., Sergeev, E., Bolognini, D., Sprenger, R.R., Ekberg, J.H., Ejsing, C.S., McKenzie, C.J., Rexen Ulven, E., Milligan, G., and Ulven, T. (2018). Discovery of a potent thiazolidine free fatty acid receptor 2 agonist with favorable pharmacokinetic properties. J. Med. Chem. *61*, 9534–9550.

Hassane, M., Demon, D., Soulard, D., Fontaine, J., Keller, L.E., Patin, E.C., Porte, R., Prinz, I., Ryffel, B., Kadioglu, A., et al. (2017). Neutrophilic NLRP3 inflammasome-dependent IL-1β secretion regulates the γδT17 cell response in respiratory bacterial infections. Mucosal Immunol. *10*, 1056–1068.

Horvat, J.C., Beagley, K.W., Wade, M.A., Preston, J.A., Hansbro, N.G., Hickey, D.K., Kaiko, G.E., Gibson, P.G., Foster, P.S., and Hansbro, P.M. (2007). Neonatal chlamydial infection induces mixed T-cell responses that drive allergic airway disease. Am. J. Respir. Crit. Care Med. *176*, 556–564.

Hudson, B.D., Christiansen, E., Murdoch, H., Jenkins, L., Hansen, A.H., Madsen, O., Ulven, T., and Milligan, G. (2014). Complex pharmacology of novel allosteric free fatty acid 3 receptor ligands. Mol. Pharmacol. *86*, 200–210.

Ichinohe, T., Pang, I.K., Kumamoto, Y., Peaper, D.R., Ho, J.H., Murray, T.S., and Iwasaki, A. (2011). Microbiota regulates immune defense against respiratory tract influenza A virus infection. Proc. Natl. Acad. Sci. USA *108*, 5354–5359.

Kjos, M., Aprianto, R., Fernandes, V.E., Andrew, P.W., van Strijp, J.A.G., Nijland, R., and Veening, J.-W. (2015). Bright fluorescent Streptococcus pneumoniae for live-cell imaging of host-pathogen interactions. J. Bacteriol. *197*, 807–818.

Koh, A., De Vadder, F., Kovatcheva-Datchary, P., and Bäckhed, F. (2016). From dietary fiber to host physiology: short-chain fatty acids as key bacterial metabolites. Cell *165*, 1332–1345.

Lankelma, J.M., Birnie, E., Weehuizen, T.A.F., Scicluna, B.P., Belzer, C., Houtkooper, R.H., Roelofs, J.J.T.H., de Vos, A.F., van der Poll, T., Budding, A.E., and Wiersinga, W.J. (2017). The gut microbiota as a modulator of innate immunity during melioidosis. PLoS Negl. Trop. Dis. *11*, e0005548.

Levy, M., Kolodziejczyk, A.A., Thaiss, C.A., and Elinav, E. (2017). Dysbiosis and the immune system. Nat. Rev. Immunol. *17*, 219–232.

Li, G., Xie, C., Lu, S., Nichols, R.G., Tian, Y., Li, L., Patel, D., Ma, Y., Brocker, C.N., Yan, T., et al. (2017). Intermittent fasting promotes white adipose browning and decreases obesity by shaping the gut microbiota. Cell Metab. *26*, 672–685.e4.

Macia, L., Tan, J., Vieira, A.T., Leach, K., Stanley, D., Luong, S., Maruya, M., Ian McKenzie, C., Hijikata, A., Wong, C., et al. (2015). Metabolite-sensing receptors GPR43 and GPR109A facilitate dietary fibre-induced gut homeostasis through regulation of the inflammasome. Nat. Commun. *6*, 6734.

Mancuso, P., Huffnagle, G.B., Olszewski, M.A., Phipps, J., and Peters-Golden, M. (2006). Leptin corrects host defense defects after acute starvation in murine pneumococcal pneumonia. Am. J. Respir. Crit. Care Med. *173*, 212–218.

Mariño, E., Richards, J.L., McLeod, K.H., Stanley, D., Yap, Y.A., Knight, J., McKenzie, C., Kranich, J., Oliveira, A.C., Rossello, F.J., et al. (2017). Gut microbial metabolites limit the frequency of autoimmune T cells and protect against type 1 diabetes. Nat. Immunol. *18*, 552–562.

Maslowski, K.M., and Mackay, C.R. (2011). Diet, gut microbiota and immune responses. Nat. Immunol. *12*, 5–9.

Maslowski, K.M., Vieira, A.T., Ng, A., Kranich, J., Sierro, F., Yu, D., Schilter, H.C., Rolph, M.S., Mackay, F., Artis, D., et al. (2009). Regulation of inflammatory responses by gut microbiota and chemoattractant receptor GPR43. Nature *461*, 1282–1286.

McAleer, J.P., and Kolls, J.K. (2018). Contributions of the intestinal microbiome in lung immunity. Eur. J. Immunol. *48*, 39–49.

McCullers, J.A. (2014). The co-pathogenesis of influenza viruses with bacteria in the lung. Nat. Rev. Microbiol. *12*, 252–262.

McNamee, L.A., and Harmsen, A.G. (2006). Both influenza-induced neutrophil dysfunction and neutrophil-independent mechanisms contribute to increased susceptibility to a secondary Streptococcus pneumoniae infection. Infect. Immun. *74*, 6707–6721.

Milligan, G., Shimpukade, B., Ulven, T., and Hudson, B.D. (2017). Complex pharmacology of free fatty acid receptors. Chem. Rev. *117*, 67–110.

Monto, A.S., Gravenstein, S., Elliott, M., Colopy, M., and Schweinle, J. (2000). Clinical signs and symptoms predicting influenza infection. Arch. Intern. Med. *160*, 3243–3247.

Moriyama, M., and Ichinohe, T. (2019). High ambient temperature dampens adaptive immune responses to influenza A virus infection. Proc. Natl. Acad. Sci. USA *116*, 3118–3125.

Nakamatsu, M., Yamamoto, N., Hatta, M., Nakasone, C., Kinjo, T., Miyagi, K., Uezu, K., Nakamura, K., Nakayama, T., Taniguchi, M., et al. (2007). Role of interferon-gamma in Valpha14+ natural killer T cell-mediated host defense against Streptococcus pneumoniae infection in murine lungs. Microbes Infect. *9*, 364–374.

Paget, C., and Trottein, F. (2019). Mechanisms of bacterial superinfection post-influenza: a role for unconventional T cells. Front. Immunol. *10*, 336.

Paget, C., Ivanov, S., Fontaine, J., Blanc, F., Pichavant, M., Renneson, J., Bialecki, E., Pothlichet, J., Vendeville, C., Barba-Spaeth, G., et al. (2011). Potential role of invariant NKT cells in the control of pulmonary inflammation and CD8+ T cell response during acute influenza A virus H3N2 pneumonia. J. Immunol. *186*, 5590–5602.

Planet, P.J., Parker, D., Cohen, T.S., Smith, H., Leon, J.D., Ryan, C., Hammer, T.J., Fierer, N., Chen, E.I., and Prince, A.S. (2016). Lambda interferon restructures the nasal microbiome and increases susceptibility to Staphylococcus aureus superinfection. mBio *7*, e01939, e15.

Qin, N., Zheng, B., Yao, J., Guo, L., Zuo, J., Wu, L., Zhou, J., Liu, L., Guo, J., Ni, S., et al. (2015). Influence of H7N9 virus infection and associated treatment on human gut microbiota. Sci. Rep. *5*, 14771.

Rynda-Apple, A., Robinson, K.M., and Alcorn, J.F. (2015). Influenza and bacterial superinfection: illuminating the immunologic mechanisms of disease. Infect. Immun. *83*, 3764–3770.

Schuijt, T.J., Lankelma, J.M., Scicluna, B.P., de Sousa e Melo, F., Roelofs, J.J., de Boer, J.D., Hoogendijk, A.J., de Beer, R., de Vos, A., Belzer, C., et al. (2016). The gut microbiota plays a protective role in the host defence against pneumococcal pneumonia. Gut *65*, 575–583.

Shapiro, H., Thaiss, C.A., Levy, M., and Elinav, E. (2014). The cross talk between microbiota and the immune system: metabolites take center stage. Curr. Opin. Immunol. *30*, 54–62.

Short, K.R., Kroeze, E.J.B.V., Fouchier, R.A.M., and Kuiken, T. (2014). Pathogenesis of influenza-induced acute respiratory distress syndrome. Lancet Infect. Dis. *14*, 57–69.

Steed, A.L., Christophi, G.P., Kaiko, G.E., Sun, L., Goodwin, V.M., Jain, U., Esaulova, E., Artyomov, M.N., Morales, D.J., Holtzman, M.J., et al. (2017). The microbial metabolite desaminotyrosine protects from influenza through type I interferon. Science *357*, 498–502.

Sun, K., and Metzger, D.W. (2014). Influenza infection suppresses NADPH oxidase-dependent phagocytic bacterial clearance and enhances susceptibility to secondary methicillin-resistant Staphylococcus aureus infection. J. Immunol. *192*, 3301–3307.

Tan, J., McKenzie, C., Potamitis, M., Thorburn, A.N., Mackay, C.R., and Macia, L. (2014). The role of short-chain fatty acids in health and disease. Adv. Immunol. *121*, 91–119.

Thaiss, C.A., Zmora, N., Levy, M., and Elinav, E. (2016). The microbiome and innate immunity. Nature *535*, 65–74.

Trompette, A., Gollwitzer, E.S., Yadava, K., Sichelstiel, A.K., Sprenger, N., Ngom-Bru, C., Blanchard, C., Junt, T., Nicod, L.P., Harris, N.L., and Marsland, B.J. (2014). Gut microbiota metabolism of dietary fiber influences allergic airway disease and hematopoiesis. Nat. Med. *20*, 159–166.

Trompette, A., Gollwitzer, E.S., Pattaroni, C., Lopez-Mejia, I.C., Riva, E., Pernot, J., Ubags, N., Fajas, L., Nicod, L.P., and Marsland, B.J. (2018). Dietary fiber confers protection against flu by shaping $Ly6c^{-}$ patrolling monocyte hematopoiesis and $CD8^{+}$ T cell metabolism. Immunity *48*, 992–1005.e8.

Ulven, T. (2012). Short-chain free fatty acid receptors FFA2/GPR43 and FFA3/GPR41 as new potential therapeutic targets. Front. Endocrinol. (Lausanne) *3*, 111.

van der Poll, T., and Opal, S.M. (2009). Pathogenesis, treatment, and prevention of pneumococcal pneumonia. Lancet *374*, 1543–1556.

Wang, J., Li, F., Wei, H., Lian, Z.-X., Sun, R., and Tian, Z. (2014a). Respiratory influenza virus infection induces intestinal immune injury via microbiota-mediated Th17 cell-dependent inflammation. J. Exp. Med. *211*, 2397–2410.

Wang, Y., Dai, A., Huang, S., Kuo, S., Shu, M., Tapia, C.P., Yu, J., Two, A., Zhang, H., Gallo, R.L., and Huang, C.M. (2014b). Propionic acid and its esterified derivative suppress the growth of methicillin-resistant Staphylococcus aureus USA300. Benef. Microbes *5*, 161–168.

Yildiz, S., Mazel-Sanchez, B., Kandasamy, M., Manicassamy, B., and Schmolke, M. (2018). Influenza A virus infection impacts systemic microbiota dynamics and causes quantitative enteric dysbiosis. Microbiome *6*, 9.

Zelaya, H., Alvarez, S., Kitazawa, H., and Villena, J. (2016). Respiratory antiviral immunity and immunobiotics: beneficial effects on inflammation-coagulation interaction during influenza virus infection. Front. Immunol. *7*, 633.

STAR★METHODS

KEY RESOURCES TABLE

REAGENT or RESOURCE	SOURCE	IDENTIFIER
Antibodies		
mAb anti-CD45 (BV510)	BioLegend	Cat# 103138, clone 30-F11, RRID: AB_2563061
mAb anti-CD11b (perCP/Cy5.5)	BioLegend	Cat# 101228, clone M1/70, RRID: AB_893232
mAb anti-Ly6G (APC-Cy7)	BioLegend	Cat# 127624, clone 1A8, RRID: AB_10640819
mAb anti-Siglec F (PE)	BD Biosciences	Cat# 552126, clone E50-2440, RRID: AB_394341
mAb anti-CD11c (PE/Cy7)	BioLegend	Cat# 117318, clone N1418, RRID: AB_493568
mAb anti-MHCII (AF700)	BioLegend	Cat# 107622, clone M5/114.15.2, RRID: AB_493727
mAb anti-CD64 (APC)	BioLegend	Cat# 139306, clone X54-5/7.1, RRID: AB_11219391
mAb anti-TCRb (Pe/Cy7)	BioLegend	Cat# 109222, clone H57-597, RRID: AB_893625
mAb anti-CD11b (PerCP/Cy5.5)	BioLegend	Cat# 101228, clone M1/70, RRID: AB_893232
mAb anti-IFNg (AF647)	BioLegend	Cat# 505814, clone XMG1.2, RRID: AB_493314
mAb anti-IL17A (PE)	BioLegend	Cat# 506904, clone TC11-18H10.1, RRID: AB_315464
Bacterial and Virus Strains		
Influenza A/ Scotland/ 20/ 74 (H3N2) virus	(Barthelemy et al., 2017)	N/A
Influenza A/California/04/2009	(Barthelemy et al., 2018)	N/A
Influenza A/WSN/1933 (H1N1) virus	(Barthelemy et al., 2017)	N/A
Streptococcus pneumoniae clinical isolate E1586 (serotype 1)	(Barthelemy et al., 2017)	N/A
Streptococcus pneumoniae eGFP	(Kjos et al., 2015)	N/A
Chemicals and Antibiotics		
Propidium iodide	BioLegend	Cat# 421301
Power SYBR Green PCR Master Mix	ThermoFisher Scientific	Cat# 4367660
Neomycin	Sigma-Aldrich	Cat# N6386
Ciprofloxacin	Sigma-Aldrich	Cat# 17850
Ampicillin	Sigma-Aldrich	Cat# M3761
Metronidazole	Sigma-Aldrich	Cat# N6386
Nystatin	Sigma-Aldrich	Cat# N40014
Vancomycin	R&D	Cat# 5506
Gentamicin	ThermoFisher Scientific	Cat# 15710049
Sodium Acetate	Sigma-Aldrich	Cat# 791741
CellMask Green Plasma Membrane Stain	ThermoFisher Scientific	Cat# C37608
DAPI	ThermoFisher Scientific	Cat# D1306
Thioglycollate Broth	Sigma-Aldrich	Cat# 70157
Clodronate liposome	Liposoma	Cat# CP-005-005
Critical Commercial Assays		
High-Capacity RNA-to-cDNA Kit	ThermoFisher Scientific	Cat# 4387406
NucleoSpin® RNA	Macherey-Nagel	Cat# 740955
QIAamp DNA Stool Mini Kit	QIAGEN	Cat# 51504
MetaBiote®	Genoscreen	N/A
AMPure XP	Beckman Coulter	Cat# A63880
Experimental Models: Organisms/Strains		
Mouse: C57BL/6J	Janvier Labs, France	RRID:MGI:5752053
Ffar2$^{-/-}$	(Maslowski et al., 2009)	N/A

(*Continued on next page*)

Continued

REAGENT or RESOURCE	SOURCE	IDENTIFIER
Deposited data		
16S ribosomal gene sequences dataset	This paper	NCBI: PRJNA602797
Oligonucleotides		
GAPDH Forward 5′-GCAAAGTGGAGATTGTTGCCA-3′ Reverse 5′-GCCTTGACTGTGCCGTTGA-3′	This study	N/A
Oas3 Forward 5′-GTGGCACCGATGTCGAACTC-3′ Reverse 5′-AGCAACATTCGCATGGCA-3′	This study	N/A
Stat1 Forward 5′-GCTGCCTATGATGTCTCGTTTG-3′ Reverse 5′-TTCCGTATGTTGTGCTGCAAC-3′	This study	N/A
FoxJ1 Forward 5′-CCACCAAGATCACTCTGTCGG-3′ Reverse 5′-AGGACAGGTTGTGGCGGAT-3′	This study	N/A
Occluding Forward 5′-AGCAGCCCTCAGGTGACTGTTATT-3′ Reverse 5′-ACGACGTTAACTCCTGAACAAGCA-3′	This study	N/A
VE-cacherin (Cdh5) Forward 5′-AGAGTCCATCGCAGAGTC-3′ Reverse 5′-CAGCCAGCATCTTGAACC-3′	This study	N/A
Isg15 Forward 5′-GGCCACAGCAACATCTATGAGG-3′ Reverse 5′-CTCGAAGCTCAGCCAGAACTG-3′	This study	N/A
Ffar2 Forward 5′- TTAATCTGACCCTGGCGGAC-3′, Reverse 5′-AGCGCGCACACGATCTTT-3′,	This study	N/A
Ffar3 Forward 5′-TTGTATCGACCCCCTGGTTTT-3′ Reverse 5′-GCTGAGTCCAAGGCACACAAG-3′	This study	N/A
IAV M1 Forward 5′-AAGAACAATCCTGTCACCTC TGA −3′ Reverse 5′-CAAAGCGTCTACGCTGCAGTCC-3′	This study	N/A
Table S6		
Software and Algorithms		
GraphPad Prism	GraphPad Software	https://www.graphpad.com
FACSDiva	BD FACSDIVA™ Software	N/A
FLASH		N/A
QIIME v1.9.1	QIIME	http://qiime.org/
Uclust v1.2.22q		N/A
RDP classifier method v2.2		N/A
Primer Express Software v3.0.1	ThermoFisher Scientific	Cat# 4363991
ZEN	Zeiss	https://www.zeiss.fr/corporate/home.html
AutoQuant	Bitplane	https://imaris.oxinst.com
ImageJ	ImageJ	https://imagej.nih.gov/ij/
Others		
Standard diet	Safe	Cat# U8231G10R

LEAD CONTACT AND MATERIALS AVAILABILITY

Further information and requests for resources and reagents should be directed to and will be fulfilled by the Lead Contact, François Trottein (francois.trottein@pasteur-lille.fr).

This study did not generate new unique reagents.

EXPERIMENTAL MODEL AND SUBJECT DETAILS

Mice and ethics statement

Specific pathogen-free C57BL/6J mice (6 week-old, male) were purchased from Janvier (Le Genest-St-Isle, France). Mice were maintained in a biosafety level 2 facility in the Animal Resource Center at the Lille Pasteur Institute for at least two weeks prior to usage

to allow appropriate acclimatation. All experiments complied with current national and institutional regulations and ethical guidelines (Institut Pasteur de Lille/B59-350009 and CEEA 75. Nord Pas-de-Calais). All experiments were approved by the Ministère de l'Education Nationale, de l'Enseignement Supérieur et de la Recherche, France (00357.03 and APAFIS 13743-2018022211144403). *Ffar2*$^{-/-}$ mice (> 10 backcrosses) were produced as previously described (Maslowski et al., 2009).

Viruses and bacteria

The mouse-adapted H3N2 IAV strain Scotland/20/1974, H1N1 IAV strain WSN/1933, H1N1 IAV strain California/04/2009 (pdm09), and the clinical *S. pneumoniae* isolate E1586 (serotype 1) were described in Barthelemy et al. (2018).

METHOD DETAILS

Diets

Unless specified, mice were fed a standard rodent chow (SAFE A04) (SAFE, Augy, France) and water *ad libitium*. This diet contains ~11.8% fiber including ~10% water-insoluble fiber (3.6% cellulose) and 1.8% water-soluble fiber.

Infections and assessment of bacterial loads

For infection with IAV alone, mice were anesthetized by intramuscular injection of 1.25 mg of ketamine plus 0.25 mg of xylazine in 100 μl of phosphate buffered saline (PBS), and then intranasally (i.n.) infected with 50 μl of PBS containing (or not, in a mock sample) 30 plaque forming units (p.f.u.) of the H3N2 IAV strain A/Scotland/20/1974, 200 p.f.u. of the H1N1 IAV strain A/WSN/1933 or 100 p.f.u. of H1N1 A/California/04/2009 (pdm09) (Barthelemy et al., 2017, 2018). These doses correspond to sub-lethal doses, which are necessary to investigate secondary bacterial infection. For infection with *S. pneumoniae* alone, a high dose ($1x10^6$ c.f.u.) of *S. pneumoniae* serotype 1, a serotype linked to invasive pneumococcal disease (clinical isolate E1586) was used. To deplete alveolar macrophages, mice were i.n. inoculated with empty liposomes or clodronate liposomes (50μl, Liposoma, Amsterdam, the Netherlands) 24 h before the *S. pneumoniae* challenge. For secondary pneumococcal infection, IAV (H1N1, pdm2009)-infected mice were challenged at 7 dpi with a low dose ($1x10^3$ c.f.u.) of *S. pneumoniae*, a dose that is largely sufficient to allow bacterial outgrowth and dissemination. In single and double infected mice, bacteria in the lungs and spleen were counted 30 h after the *S. pneumoniae* challenge by plating serial 10-fold dilutions of lung or spleen homogenates onto blood agar plates. The plates were incubated at 37°C with 5% CO_2 overnight and viable bacteria were counted 24 h later. Survival and *body weight* were monitored daily after IAV infection and mice were euthanized when they lost in excess of 20% of their initial body weight.

Reagents, antibodies, flow cytometry and cell sorting

The FFAR2 agonist TUG-1375 (2*R*,4*R*)-2-(2-chlorophenyl)-3-(4-(3,5-dimethylisoxazol-4-yl)benzoyl)thiazolidine-4-carboxylic acid) and the FFAR3 agonist AR420626 (*N*-(2,5-dichlorophenyl)-4-(furan-2-yl)-2-methyl-5-oxo-1,4,5,6,7,8-hexahydroquinoline-3-carboxamide were produced as described (Hansen et al., 2018; Hudson et al., 2014). Acetate, propionate and butyrate were from Sigma-Aldrich (Saint Louis, MO). Ampicillin, neomycin, metronidazole, ciprofloxacinand and nystatin were from Sigma-Aldrich and vancomycin was from R&D systems (Minneapolis, MN). Antibodies used for flow cytometry have been described in Barthelemy et al. (2016, 2017). Flow cytometry analysis was performed exactly as described (Barthelemy et al., 2016). Monoclonal antibodies against mouse CD45 (Brilliant Violet 510-conjugates), CD11b (PerCP-Cy5.5-conjugated), Siglec F (PE-conjugated), Ly6G (APC-H7-conjugated), CD11c (PE-Cy7-conjugated), MHC class II (AF700-conjugated), CD64 (APC-conjugated), TCRβ (PE-Cy7-conjugated), TCRγδ (PerCP-Cy5.5-conjugated), IFN-γ (AlexaFluor-647), IL-17A (PE), and isotype controls were purchased from BioLegend (San Diego, USA) and BD Bioscience (New Jersey, USA). PBS-57 glycolipid-loaded and unloaded control CD1d tetramers (APC-conjugated) were from the National Institute of Allergy and Infectious Diseases Tetramer Facility (Emory University, Atlanta, GA). The propidium iodide was purchased from BioLegend (San Diego, CA).

Cell immunostaining and flow cytometry were performed as previously described (Barthelemy et al., 2017). Briefly, mononuclear cells from the lungs were plated in U-bottom 96-well plates and labeled for dead cells (ThermoFisher Scientific). To identify immune cells, lung mononuclear cells were labeled with appropriate dilutions of conjugated antibodies exactly as described (Barthelemy et al., 2017). The data were acquired on an LSRFortessa cytometer (Becton Dickinson Biosciences, Rungis, France) running *FACSDiva* software and were then analyzed with *FACSDiva* software. For the analysis, $1x10^6$ cells were acquired. Macrophages were identified as CD45$^+$ Siglec F$^+$ CD11b^{low} and neutrophils as CD45$^+$ CD11b$^+$ Ly6G$^+$ Siglec F$^-$. Conventional dendritic cells were identified as CD45$^+$ CD11c^{+high} MHC class II$^+$ Siglec F$^-$ CD64$^-$, monocyte derived dendritic cells as CD45$^+$ CD11c$^+$ MHCII$^+$ Cd11b$^+$ Siglec F$^-$ Ly6G$^-$ CD64$^+$, γδ T cells as CD45$^+$ TCRβ$^-$ TCRγδ$^+$ and invariant natural killer T as CD45$^+$ TCRβ$^+$ CD1d tetramer$^+$. Intracellular FACS staining of *i*NKT cells and γδ T cells was performed as described (Barthelemy et al., 2017; Hassane et al., 2017). After cell surface labeling, alveolar macrophages were sorted using a FACSAria cytometer (BD Biosciences).

Sample collection, DNA extraction and 16S rRNA gene copy number

To study the impact of influenza infection on the gut microbiota, mice were i.n. infected with IAV and their feces were collected at 7 dpi and 14 dpi. Feces from each mouse were also sampled the day of infection (one hour before IAV infection) and served as controls. Cecal samples were collected from different sets of animals including mock-treated mice and IAV-infected (7 dpi and 14 dpi) mice.

Fecal samples from vehicle-treated and acetate-treated mice were also collected at 7 dpi. Fecal and cecal samples as well as whole cecum homogenates were stored at −80°C until further analysis. Microbial DNA was extracted from 150 mg of fecal or cecal samples (QIAamp DNA stool Kit, QIAGEN, Germany). The concentration of extracted DNA was determined using on a DNA fluorometric intercalant (SYBR® Green, ThermoFisher Scientific (Waltham, MA)). Bacterial loads were quantified using qPCR assays. Standard curves were constructed to optimize the experiments and perform absolute quantification. The standard was a mix of 17 genomic DNA extracted from different bacterial strains with an even 16S rRNA gene copy number of each strain. Briefly 4.8 μl (1 ng DNA) were added into 10 μl of total volume mix (Taqman Universal MasterMix, Thermofischer) and optimized primer/probe concentrations to obtain a 100 ± 10% qPCR efficiency on the standard and samples. Cycling condition were those recommended by the manufacturer. Each sample was analyzed in triplicates. The Ct values were calculated using default parameters of software provided by the real-time PCR instrument manufacturers (7900HT fast real-time PCR System, Thermofischer). Mean Ct values were finally confronted to the standard curve to deduce the number of 16S rRNA gene copy in each sample.

16S rRNA gene pyrosequencing and data processing

The V3-V4 region of the 16S rRNA gene was amplified using an optimized and standardized amplicon-library preparation protocol (Metabiote®, GenoScreen, Lille, France). Positive (artificial bacteria Community comprising 17 different bacteria (ABCv2)) and negative (sterile water) control were also included. Briefly, PCR reactions were performed using 5ng of genomic DNA and in-house fusion barcoded primers (at 0.2 μM final concentrations), with an annealing temperature of 50°C for thirty cycles. PCR products were purified using Agencourt AMPure XP magnetic beads (Beckman Coulter, Brea, CA, USA), quantified according to GenoScreen's protocol, and mixed in an equimolar amount. Sequencing was performed using 250-bp paired-end sequencing chemistry on the Illumina MiSeq platform (Illumina, San Diego, CA, USA). Raw paired-end reads were then demultiplexed per sample and subjected to the following process: (1) search and removal of both forward and reverse primer using CutAdapt, with no mismatches allowed in the primers sequences; (2) quality-filtering using the PRINSEQ-lite PERL script, by truncating bases at the 3′ end with Phred quality score < 30; (3) paired-end read assembly using FLASH, with a minimum overlap of 30 bases and > 97% overlap identity.

Taxonomic Affiliation and diversity analyses

Taxonomic and diversity analyses were performed with the Metabiote Online v2.0 pipeline (GenoScreen, Lille, France) that is partially based on the software QIIME v1.9.1. Following the pre-processing, the full-length 16S rRNA sequences were analyzed and chimeric sequences were removed from the dataset (in-house method based on the use of USEARCH8.1 algorithm). Then, a clustering step was performed in order to group similar sequences with a nucleic identity defined threshold (97% identity for an affiliation at the genus level on the V3-V4 regions of the 16S rRNA gene) with Uclust v1.2.22q through an open-reference operational taxonomic unit (OTU) picking process and complete-linkage method, finally creating groups of sequences or OTUs. An OTU cleaning step based on the data obtained for the ABCv2 community was performed. The most abundant sequence of each OTU was considered as the reference sequence of its OTU and was then taxonomically compared to a reference database (Greengenes database, release 13_8; https://greengenes.secondgenome.com/) by the RDP classifier method v2.2. Various diversity indices were computed using QIIME v1.9.1. Alpha diversity indices (within-sample) and beta diversity (between-sample) were used to examine changes in microbial community structure between mice fecal and cecal group samples. Measurement of alpha diversity included Shannon diversity index, number of observed OTUs and Chao1 index (richness and evenness). For β-diversity measures, we computed the weighted UniFrac distances. The principal coordinates analysis (PCoA) method was used to visualize group overall microbial differences. Differences in relative abundance of individual taxa, between mice cecal group samples, were assessed for significance using the Mann-Whitney *U* test controlling for false-discovery rate (FDR), implemented within the software package QIIME. The Wilcoxon signed-rank test (paired t test) was used for 16S analysis of fecal samples.

Measurement of food consumption and pair-feeding experiments

Food consumption was calculated daily during influenza infection. Briefly, a known amount of food was placed in a cage of six mice. The amount of remaining food was measured every 12 h. The amount of consumed food was calculated by the difference divided by six and expressed as food intake per mouse per day. To provide the pair-fed group with only as much food daily as is consumed by IAV-infected mice, we restricted the food access during the last three days for 15% (day 4), 35% (day 5) and 85% (day 6), respectively (sacrifice at day 7). Mice were anesthetized at day 0. The pair-feeding time point was determined using data generated from IAV-infected mice with the goal of achieving a ∼15% loss of body mass (as at 7 dpi). Food was supplied twice a day to pair-fed animals and water was available at all times. The *ad libitum* (normally nourished) group mice were allowed unrestricted access to food and water. Weight loss of paired-fed mice and IAV-infected mice were measured in a daily manner. Fecal pellets (16S rRNA sequencing) and cecal content (SCFA quantification) were collected at baseline (control) and seven days after (pair fed).

Measurement of SCFA concentrations and treatment with acetate or FFAR2/FFAR3 agonists

Concentrations of SCFAs in the cecal content were determined after extraction with diethyl ether using GC-2014 gas chromatography with AOC-20i auto injector (Shimadzu, Hertogenbosch, the Netherlands) as described (De Weirdt et al., 2010). Concentrations of SCFAs in plasma were determined after extraction with acetonitrile. Results are expressed as μmol/g of cecal content or as μM (blood). To assess the effects of SCFAs on lung defense against bacterial infection, conventional mice (no ABX treatment), mice

recolonized with IAV microbiota and mice infected with IAV were treated with acetate (200 mM, drinking water) five days before the *S. pneumoniae* challenge ($1x10^6$ c.f.u. for conventional and recolonized mice and $1x10^3$ c.f.u. for IAV-infected mice, respectively). IAV-infected mice were also treated (drinking water) with a combination of acetate, propionate and butyrate (200mM, 50mM and 5mM, respectively). The FFAR2 agonist TUG-1375 and the FFAR3 agonist AR420626 (stock solutions in DMSO at 20mM) were inoculated by the i.n. route (50 μl, 1 mM) 16 h before *S. pneumoniae* infection. Histopathological evaluation of the lung of double-infected mice was performed as described previously (Horvat et al., 2007).

Quantification of viral loads and assessment of gene expression by quantitative RT-PCR

Total RNA from lung tissues were extracted with the NucleoSpin® RNA kit (Macherey-Nagel, Hoerdt, Germany). RNA was reverse-transcribed with the High-Capacity cDNA Archive Kit (Life Technologies, USA). The resulting cDNA was amplified using SYBR Green-based real-time PCR and the QuantStudio 12K Flex Real-Time PCR Systems (Applied Biosystems, USA) following manufacturers protocol. Relative quantification was performed using the gene coding glyceraldehyde 3-phosphate dehydrogenase (*Gapdh*). Specific primers were designed using Primer Express software (Applied Biosystems, Villebon-sur-Yvette, France) and ordered to Eurofins Scientifics (Ebersberg, Germany). Relative mRNA levels ($2^{-\Delta\Delta Ct}$) were determined by comparing (a) the PCR cycle thresholds (Ct) for the gene of interest and the house keeping gene *Gadph* (ΔCt) and (b) ΔCt values for treated and control groups (ΔΔCt). Data are expressed as a fold-increase over the mean gene expression level in mock-treated mice. Quantification of viral RNA was performed as described in Paget et al. (2011). Viral load is expressed as viral RNA normalized to *gapdh* expression level. Data were normalized against expression of the *gapdh* gene and were expressed as Ct.

Microbiota transfer experiments

Mice received broad-spectrum ABXs (ampicillin 2g/L; neomycin 2g/L, metronidazole 1g/l, ciprofloxacin 1g/l, nystatin 0.08 g/L and vancomycin 0.5g/l) in drinking water supplemented with glucose (10 g/l) for three weeks. The cages were changed every two days. Depletion of bacteria in the feces were checked after culture in thioglycollate broth medium (Sigma) for 24 h at 37°C. ABX-treated mice were colonized twice (three days and five days after ABX cessation) by oral administration of 200 μl of cecal suspension containing $1x10^9$ bacteria recovered from naive mice, mock-treated mice or IAV-infected mice (7 dpi). Colonized mice were infected with *S. pneumoniae* ($1x10^6$ c.f.u.) three days after the first colonization. Weights of control and ABX-treated mice (colonized or not) were equal at the moment of pneumococcal inoculation.

In vivo phagocytosis and killing assays and assessment of pneumococcal load in alveolar macrophages

To visualize bacteria associated with phagocytes or internalized by phagocytes, recolonized mice were infected with eGFP-expressing *S. pneumoniae* ($1x10^6$ c.f.u., serotype 1) (a gift from Dr JW Veening, university of Groningen, the Netherlands). Four hours later, BAL fluid cells (> 95% alveolar macrophages) were washed and plated (u-Slide 8 Well ibiTreat, IBIDI, Martinsried, Germany). Membranes were labeled (CellMaskDeep red plasma membrane stain, Thermofisher) and after washes and fixation, nucleus were labeled with DAPI (Thermofisher) and maintained in PBS. Samples were observed with CLSM Zeiss LSM 880 (Zeiss, Oberkochen, Germany) with Plan Apochromat 63xoil/1.4 objective. Excitation was performed with an Argon laser (458 to 488 to 514 nm) or a laser diode (561 nm and 405nm) (Lasos Lasertechnik GmbH, Jena, Germany). The spectral detection range was adjusted for each fluorophore by using a Quasar detection unit. Images were acquired with ZEN software (Zeiss, Carl Zeiss, Oberkochen, Germany), deconvoled by AutoQuant software (Bitplane, Oxford Instruments company, Zurich, Switzerland) and assembled using ImageJ software. The frequency of macrophages having internalized *S. pneumoniae* and the average number of internalized bacteria per macrophage were determined (more than 20 visual fields analyzed/mouse). To determine the pneumococcal load in alveolar macrophages, cells ($CD45^+$ Siglec F^{hi} $CD11b^-$) were sorted using a FACSAria cytometer (BD Biosciences) (> 99% purity). DNA was extracted and analyzed using quantitative PCR (QuantStudio 12K Flex, Applied Biosystems). Data were normalized against expression of the *gapdh* gene and were expressed as ΔCt. To determine the bactericidal activity of macrophages, re-colonized mice were infected with $1x\ 10^6$ c.f.u. of *S. pneumoniae* (serotype 1). Four hours later, BAL fluid cells were collected and extensively washed with PBS in the presence of 15 μg/ml of gentamycin (Thermo Fisher Scientific). Cells were then washed twice in sterile PBS and lysed in sterile double deionized water. To assess bacterial killing, the number of ingested viable bacteria was determined by quantitative plating of serial dilutions of the lysates onto blood agar plates. The number of viable bacteria was expressed per $1x10^5$ cells.

In vitro killing assay

For the *in vitro* killing assay, macrophages were pre-treated with acetate (10mM) for 1 h and then exposed with opsonized *S. pneumoniae* at MOI 10. Cells were incubated at 4°C for 1 h, followed by 3h of incubation at 37°C for bacterial internalization. Cells were washed in sterile PBS, incubated with penicillin and streptomycin (30U/ml) for 30min to kill extracelllular bacteria and then washed and incubated with vancomycin (0.75μg/ml) for 2 h. Bacterial-exposed macrophages were lysed at 0 and 2 h post exposure. The number of viable bacteria were determined by quantitative plating of serial dilutions of the lysates onto blood agar plates.

S. pneumoniae outgrowth *in vitro*

S. pneumoniae colonies at exponential growth were added to Todd Hewitt Broth at the absorbance of 0.04 OD (600 nm) in the absence or presence of 0.1, 1 or 10mM of acetate, or 1U/ml of pennicilin and 1 μg/ml streptomycin used here as a positive control. The O.D. was measured every 30 minutes.

QUANTIFICATION AND STATISTICAL ANALYSIS

Results are expressed as the mean ± standard deviation (SD) unless otherwise stated. All statistical analysis was performed using GraphPad Prism v6 software. A Mann-Whitney *U* test was used to compare two groups unless otherwise stated. The Wilcoxon signed-rank test (paired t test) was used for 16S analysis of fecal samples. Comparisons of more than two groups with each other were analyzed with the One-way ANOVA Kruskal-Wallis test (nonparametric), followed by the Dunn's posttest. Survival of mice was compared using Kaplan-Meier analysis and log-rank test.*, $p < 0.05$; **, $p < 0.01$; ***, $p < 0.001$. Statistical details of experiments can be found in the figure legends. Sample sizes were dictated to adhere to the French home office 3R principles, while providing appropriate statistical power.

DATA AND CODE AVAILABILITY

The 16S ribosomal gene sequences datasets generated during this study are available at NCBI (SRA) under accession number PRJNA602797.